

**Changes in Oriented Strandboard Permeability during Hot-Pressing**

By

Jonathan Patrick Hood

Masters Thesis submitted to the

Faculty of Virginia Polytechnic Institute and State University

in partial fulfillment of the requirements for the degree of:

Master of Science

In

Wood Science and Forest Products

Dr. Frederick A. Kamke, Chairman

Dr. Joseph R. Loferski

Dr. Audrey Zink-Sharp

July, 2004

Blacksburg, Virginia

Keywords: permeability, compaction ratio, density, Darcy's law

# Changes in OSB Mat Permeability during Hot-Pressing

Jonathan Hood

(Abstract)

Convective heat transfer during hot pressing in wood-based composite panel manufacturing is widely accepted as the most important means of heat transport for resin curing. The rate of convective heat transfer to the panel core is controlled by its permeability. Permeability in the plane of the panel also controls the flow of vapor to the panel edges, thereby influencing the potential for panel “blowing”.

This research considers how flake thickness, flake alignment and changing mat density during hot-pressing influences OSB mat permeability, through its thickness and in the plane of the panel. Some previous research exists but it fails to address the affects of horizontal and vertical density gradients as well as flake alignment.

An apparatus was designed to allow cold pressing of aligned flakes to desired densities while enabling permeability measurements through the mat thickness. An additional apparatus was designed to allow the measuring of permeability in the plane of the mat. These designs permitted permeability measurements in mats that had no vertical density gradient, allowing for the direct study of permeability versus density (compaction ratio).

Superficial permeability was determined using Darcy’s law and for each sample, multiple readings were made at five different pressure differentials. Permeability through the mat thickness was highly dependent on compaction ratio and to a lesser extent flake thickness. As the compaction ratio is increased, the initial reduction in permeability is severe, once higher compaction ratios are achieved the reduction in permeability is less pronounced. Permeability decreased with decreasing flake thickness. Permeability in the plane of the mat decreases with increasing compaction ratio but in a less severe manner than through the mat thickness. In this case, the permeability-compaction ratio relationship appears linear in nature. Again, permeability decreases with decreasing flake thickness.

## Acknowledgements

I would like to thank the many people who have helped me during my time here at Virginia Tech. Thank you to my committee members Dr. Joseph Loferski and Dr. Audrey Zink-Sharp who even outside their roles as committee members helped me learn and made me a better student. My committee chair Dr. Frederick Kamke gave me this opportunity and I learned more under his guidance than I thought possible for that, I will always be grateful.

Successful completion of this project would not have been possible without the staff in the Wood Science department. Thank you to Linda Caudill for the advice and to Rick Caudill, Kenny Albert and Butch Sizemore for the help I received. I especially want to thank Jim Fuller, without his help and design advice I would have struggled, gone home early, and given up. David Jones provided a much-needed break from the technical world as well as help on my project in many ways. Matt Reynolds, Patrick Rappold, Paul Duvall, and Jeff Smith provided sports talk and world event opinions that made the days easier.

My wife Nikol was the driving force behind this undertaking and without her I would have never made it, her encouragement and her ability to never appear bored with my shoptalk was incredible. Thanks to my parents for their belief in me and their constant support. Special thanks go to Josh Martinez who provided technical help and a strong back as well as a fishing partner, and his wife Tina Martinez provided Auto-Cad expertise. Greg and Rachel Divers also deserve my thanks for telling me I should do it and encouraging me along the way. Wherever I may end up these people will always be my dear friends.

1	Introduction and Objectives .....	1
2	Literature Review.....	3
2.1	Introduction.....	3
2.2	Permeability .....	5
2.2.1	Darcy’s Law .....	5
2.2.2	Specific Permeability .....	7
2.2.3	Flow in Wood .....	7
2.3	Heat Transport in Hot Pressing.....	9
2.3.1	Conduction.....	9
2.3.2	Convection .....	10
2.4	Permeability in Composite Pressing .....	12
2.5	Methods of Measuring Permeability.....	22
2.6	Predicting Permeability in Other Porous Media .....	24
3	Materials and Methods.....	27
3.1	Sample Preparation .....	27
3.1.1	Flake Preparation .....	27
3.1.2	In-Plane Permeability.....	28
3.1.3	Transverse Permeability.....	34
3.2	Experimental design.....	37
3.3	Apparatus .....	38
3.4	Commercial Mat Comparisons .....	40
3.5	Data Analysis.....	42
4	Results and Discussion .....	44
4.1	Transverse Permeability Results.....	44
4.1.1	Regression Analysis.....	49
4.2	In-Plane Permeability.....	52
4.2.1	In-Plane Permeability Parallel .....	53
4.2.2	In-Plan Permeability Perpendicular .....	54
4.2.3	Regression Analysis.....	56
4.3	Transverse and In-Plane Permeability Comparisons .....	59
4.4	Commercial Flake Comparison .....	62
4.5	Previous Research Comparison .....	70
5	Summary, Conclusions and Recommendations.....	74
5.1	Summary .....	74
5.2	Conclusions.....	75
5.3	Recommendations.....	76
5.4	Limitations .....	76
6	References.....	77
	Appendix.....	80

Figure 2-1. The principal directions in OSB for permeability measurements.....	13
Figure 2-2. Five period description of the mat core temperature change during the pressing operation (Bolton et al 1989a).....	18
Figure 2-3. Temperature through the mat thickness at various times during the press cycle for an 18 mm thick mat.....	19
Figure 2-4. Total gas pressure at various stages during the press cycle for an 18 mm thick mat.....	19
Figure 2-5. Moisture content at various times in pressing based on an initial face flake moisture content of 12 percent and core flake moisture content of 8 percent for an 18 mm thick mat.....	20
Figure 2-6. Apparatus for air permeability measurements (Siau 1995).....	23
Figure 3-1. Vertical density profile for 400-kg/m <sup>3</sup> mat.....	30
Figure 3-2. Vertical density profile for 640-kg/m <sup>3</sup> mat.....	31
Figure 3-3. Vertical density profile for 800-kg/m <sup>3</sup> mat.....	31
Figure 3-4. OSB sample mat restrained by plywood.....	32
Figure 3-5. In-plane permeability specimens at all five density levels increasing from left to right.....	33
Figure 3-6. In-plane permeability specimen holder.....	34
Figure 3-7. Cut away view of in-plane permeability specimen.....	34
Figure 3-8. Transverse permeability specimen holder.....	36
Figure 3-9. Detailed description of the transverse permeability box.....	36
Figure 3-10. Detailed description for the transverse permeability box lid.....	37
Figure 3-11. Apparatus design for permeability measurements in OSB mats.....	39
Figure 4-1. Superficial permeability versus compaction ratio for OSB mats comprised of 0.05 cm thick flakes. Each compaction ratio shows results from all five mats as well as the five sub-measurements.....	45
Figure 4-2. Superficial permeability versus compaction ratio for OSB mats comprised of 0.076 cm thick flakes. Each compaction ratio shows results from all five mats as well as the five sub-measurements.....	46
Figure 4-3. Superficial permeability versus compaction ratio for OSB mats comprised of 0.10 cm thick flakes. Each compaction ratio shows results from all five mats as well as the five sub-measurements.....	47
Figure 4-4. Scatter plot of actual transverse permeability measurements and predicted values for the same flake thickness based on Equation 6.....	52
Figure 4-5. In-plane permeability parallel results for all flake thicknesses investigated.....	53
Figure 4-6. In-plane permeability perpendicular results for all flake thicknesses investigated.....	55
Figure 4-7. In-plane permeability parallel actual results and predicted values for all flake thicknesses tested based on Equation 9.....	58
Figure 4-8. In-plane permeability perpendicular actual results and predicted values for the same flake thickness based on Equation 10.....	58
Figure 4-9. Between flake openings available for transverse flow.....	60
Figure 4-10. The progression from low to high compaction ratios. A. 0.28, B. 0.93, C. 1.48.....	61
Figure 4-11. An approximation of the available transverse and in-plane flowpaths.....	61

Figure 4-12. Frequency distribution of flake length for commercial flakes.....	62
Figure 4-13. Frequency distribution of flake width for commercial flakes.....	63
Figure 4-14. Frequency distribution for flake thickness of commercial flakes.....	63
Figure 4-15. Frequency distribution for flake density of commercial flakes.....	64
Figure 4-16. Commercial flake transverse permeability.....	65
Figure 4-17. Commercial flake transverse permeability results and the permeability predicted by Equation 6 for the average thickness.....	66
Figure 4-18. Commercial flake in-plane permeability parallel.....	67
Figure 4-19. Results for in-plane permeability parallel for commercial flakes and predicted permeability based on Equation 9 for average thickness.....	68
Figure 4-20. Commercial flake in-plane permeability perpendicular.....	68
Figure 4-21. Commercial flake in-plane permeability perpendicular and predicted permeability based on Equation 10 at the average flake thickness.....	69
Figure 4-22. Transverse permeability predictions based on Von Haas' equation corresponding to the range of densities commonly encountered in <i>Pinus sylvestris</i> as well as the influence of resin content (5 and 11%). Results from Equation 8 are also presented based on the same compaction ratios at a flake thickness of 0.05-cm and 0.10-cm.....	71
Figure 4-23. In-plane permeability parallel predictions based on Von Haas' equation at the high and low range end of densities commonly encountered in <i>Pinus sylvestris</i> compared to permeability predictions based on Equation 9.....	72
Figure 4-24. In-plane permeability perpendicular predictions based on Von Haas' equation at the high and low range end of densities commonly encountered in <i>Pinus</i> <i>sylvestris</i> compared to permeability predictions based on Equation 10.....	73

Table 2-1. Transverse and in-plane permeability coefficients for equation 5. ....	14
Table 3-1. Mat densities, flake thickness and number of samples for in-plane permeability determination. ....	28
Table 3-2 . Panel densities and the corresponding number of samples per flake thickness. ....	35
Table 3-3. Mat densities for in-plane permeability samples for commercial flake mats. ....	40
Table 3-4. Mat densities for transverse permeability samples for commercial flake mats. ....	41
Table 4-1. Superficial permeability ( $\text{m}^3/\text{m Pa sec}$ ) for mats comprised of 0.05-cm thick flakes. ....	48
Table 4-2. Superficial permeability ( $\text{m}^3/\text{m Pa sec}$ ) for mats comprised of 0.076-cm thick flakes. ....	48
Table 4-3. Superficial permeability ( $\text{m}^3/\text{m Pa sec}$ ) for mats comprised of 0.10-cm thick flakes. ....	48
Table 4-4. Stepwise regression results for variables entered into the model. ....	50
Table 4-5. Discriptive statistics for in-plane permeability parallel mats ( $\text{m}^3/\text{m Pa sec}$ )..	54
Table 4-6. Discriptive statistics for in-plane permeability perpendicular mats ( $\text{m}^3/\text{m Pa sec}$ ). ....	55
Table 4-7. In-plane permeability parallel summary statistics for stepwise regression. ...	57
Table 4-8. In-plane permeability perpendicular summary statistics for stepwise regression. ....	57
Table 4-9. Commercial flake descriptive statistics. ....	62

# 1 Introduction and Objectives

The purpose of this study is to determine how the transverse permeability (permeability through the mat thickness) and permeability in the plane of the mat changes during the manufacture of oriented strandboard.

The hot-pressing operation in the manufacture of wood-based composites is the most critical and most expensive step in the process. Understanding what factors influence the efficiency of hot-pressing wood-based composites can be most advantageous.

Wood-based composites are a means by which society can more efficiently utilize its natural resources. Wood-based composites can be manufactured from species, that in their solid timber form, might not be desirable for finished products. These composite products also allow the utilization of resources such as small diameter trees that would otherwise be ignored. Through the advent and further development of these products the need for the “Perfect Tree” as a requirement for a usable product has passed.

It is obvious that conductive heat transfer plays an important role in hot-pressing initially because of the direct contact between the hot platens and the oriented strandboard mats. Given the time sensitive nature of hot-pressing a total reliance on conduction would not be practical due to the slow rate of heat transfer provided by this method. So it is clear that the main ingredient in the timely curing of thermosetting adhesives is convective heat transfer based on the gas flow that occurs. Convection is strongly influenced by the

permeability of the oriented strandboard mats, which changes as the mat is consolidated. The occurrence of “blows” or areas of panel delamination at the end of hot-pressing is also directly related to the permeability of the mat.

The information gained from this research will be used to improve the Wood-Based Composite Center’s hot-pressing simulation model in the area of heat transport. It is also hoped that this research will contribute to increased efficiencies in hot-pressing oriented strandboard. It could potentially help manufacturers more efficiently plan when to inject steam during steam-injection pressing. Press closing times could be adjusted to manipulate the vertical density gradient to influence the flow in the plane of the mat.

Objectives:

1. To design and build an apparatus for measuring the transverse (through the thickness) and in-plane permeability of oriented strandboard mats during the pressing operation.
2. Determine how permeability is influenced by changes in mat density during pressing.
3. Determine what influence flake thickness and alignment have on mat permeability.
4. Develop an empirical equation that predicts permeability based on flake thickness and compaction ratio.

## **2 Literature Review**

### **2.1 Introduction**

Wood composites are a means by which the tree, as a natural resource, can be used more efficiently. Oriented strandboard (OSB) is such a composite and has become the structural panel of choice in the residential construction industry. OSB is composed of oriented layers of wood flakes with the face and back oriented in the same direction and the core arranged perpendicular to these. These flakes or strands are generally 10 cm long by 2 cm wide and 0.05-0.10 cm thick. The final panel density is approximately 500-800 kg/m<sup>3</sup>. According to the Wood Handbook, to qualify as OSB, the flake length to width ratio, or aspect ratio, must be at least 3 (Forest Products Laboratory 1999).

The OSB process consists of several key steps. Strands are cut from bolts or debarked whole logs. The strands are then dried and blended with a thermosetting adhesive. Other additives, depending on the panel end use, may be included (Forest Products Laboratory 1999). The resinated strands are formed in layers into a low-density mat, usually in a continuous manner. Using a hot-press, this low-density mat is consolidated into a much higher density final product.

Whether a continuous or multi-opening press, performs the pressing operation, what occurs is generally the same. The mat is compressed while heated. Gradually the heat from the hot platens migrates to the core, and the thermosetting adhesive polymerizes throughout the panel (Forest Products Laboratory 1999). The heat is transported by a

variety of methods, but generally it is believed that conduction and convection are the most important to this process. The rate of heat transfer is important because the adhesive requires curing temperatures above 100° C to accelerate the polymerization. This time requirement to increase the mat temperature is the main restraining factor in the production rate.

The hot-pressing operation in the manufacture of wood-based composites is the most important and most expensive step in the entire process. Wood composites get most of their final characteristics, desirable or otherwise, based on what occurs during the pressing operation. If the resin does not fully cure during the process, it is possible that, upon the release of pressure, the panel could delaminate because of expanding internal vapor pressure.

For the OSB manufacturing process to be as efficient as possible, it is important to understand the various mechanisms that affect the resin cure rate. Many of the current techniques used in the manufacturing process are based on trial and error, and do not necessarily result in the fastest cure time. The purpose of this research is to determine how mat permeability changes during the pressing operation. This will aid our understanding in what roll convection plays in the curing of the resin and in what ways it can be improved upon. This literature review will cover work done to determine what affects permeability and how it relates to the manufacture of oriented strandboard.

## 2.2 Permeability

Permeability determines the magnitude of the bulk flow of fluids through a porous medium under a pressure gradient. Many solids may be porous, but the voids must be connected for the substance to be permeable. Permeability is an important factor affecting the treatability of wood, and has been studied in extensive detail for the preservation and impregnation of wood for chemical pulping (Siau 1984). These studies have almost exclusively been limited to solid wood and static environments. This review is of studies that investigated the importance of permeability to the manufacture of wood composites and factors that influence it.

### 2.2.1 Darcy's Law

Permeability is generally described by Darcy's Law as the steady-state flow of fluids through a porous solid (Siau 1984). For an incompressible fluid (liquids) this law is described as follows:

$$k = \frac{Q/A}{\Delta P/L} = QL/A\Delta P \quad (1)$$

K = permeability,  $\text{m}^3/\text{m Pa sec}$

Q = flow rate,  $\text{m}^3/\text{sec}$

L = length of specimen in direction of flow, m

A = area perpendicular to flow direction,  $\text{m}^2$

$\Delta P$  = pressure differential over distance of flow, Pa

This equation changes when dealing with compressible (gasses) fluids. Superficial gas permeability ( $k_g$ ) is calculated as:

$$k_g = \frac{QLP}{A\Delta P\bar{P}} \quad (2)$$

$k_g$  = superficial gas permeability,  $\text{m}^3/\text{m Pa sec}$

$P$  = pressure at which flow rate is measured, Pa

$\bar{P}$  = average pressure, Pa

The compressibility of gasses and the corresponding change to the volumetric flow rate is the reason that the equation is different from that of liquids (Siau 1984).

The application of Darcy's law (Equation 1) is based on the following assumptions (Siau 1984).

1. The flow is viscous and linear, which means that the velocity and volumetric flow are directly proportional to the applied pressure differential.
2. The fluid and porous medium are homogeneous and the fluid is incompressible.
3. No interaction exists with the fluid and the medium.
4. Permeability is independent of length in the flow direction.

All of the assumptions are violated to some degree when dealing with flow in wood.

Certainly, the medium is not homogeneous. In the case of water as the fluid, there is an interaction between the fluid and the substrate. Furthermore, gasses are compressible, which can lead to continuous changes in the pressure gradient (Siau 1984). Research by (Bramhall 1970) indicates flow rate decreases exponentially with length of the flow path in wood, thus violating another assumption. Although some of these assumptions are violated when discussing the flow of air through wood, the values obtained can provide an

average permeability for each observation and provide a useful relationship between the flow rate and the pressure gradient (Siau 1984 and Joslyn 1972).

### **2.2.2 Specific Permeability**

Permeability is dependent on fluid viscosity and the porous structure of the medium. The influence of fluid viscosity is omitted by defining specific permeability ( $K$ ), which is the product of the permeability ( $k$ ) and the viscosity of the fluid. Specific permeability has the units of  $\text{m}^3/\text{m}$  or darcy and is a material property of the porous structure (Comstock 1968 and Siau 1984).

### **2.2.3 Flow in Wood**

The following types of flow in wood occur to varying degrees and can affect the validity of some of the assumptions governing Darcy's law (Siau 1984). Viscous, or laminar flow, is the flow that occurs when adjacent fluid layers overcome their friction forces and easily slide past each other. It is of primary importance to the validity of Darcy's law. Turbulent flow occurs when the viscous flow breaks down because of disturbances and requires much more energy. To overcome these disturbances the pressure differential must be increased to the point where the proportionality of flow rate to pressure differential no longer exists, thus stopping viscous flow. Turbulent flow is only encountered in long straight capillaries such as the vessels in red oak. Given the tortuous flow path encountered in most woods and wood-based composites, turbulent flow is

rarely an issue. This type of flow is encountered at Reynolds numbers higher than 2000.

The Reynolds' number is a dimensionless quantity determined by the following equation

for flow in pipes:

$$\text{Re} = \frac{2\rho Q}{\pi\mu} = \frac{d\bar{v}\rho}{\mu} \quad (3)$$

Re = Reynolds' number

$\rho$  = fluid density, kg/m<sup>3</sup>

r = radius of capillary, m

d = diameter, m

$\bar{v}$  = linear velocity, m/s

$\mu$  = fluid viscosity, Ns/m<sup>2</sup>

Nonlinear flow is encountered when kinetic energy is lost at the entrances of very small and short capillary openings, resulting in a larger energy requirement for the same rate of flow. Knudsen diffusion is the molecular diffusion through a capillary under a pressure gradient. This occurs when the capillaries are approximately the same diameter as the mean free path of the fluid molecules (Siau 1995). In Humphrey and Bolton's (1989) review of the literature they report that viscous flow is likely the only flow encountered in conventional hot-pressing. Although turbulent flow may be possible in steam injection pressing.

## **2.3 Heat Transport in Hot Pressing**

The heat transport mechanisms of conduction, convection and radiation are all believed to have some influence in the hot-pressing of wood-based composites. However, it is doubtful that radiation plays much of a roll outside of the transfer of heat from the top platen to the top of the mat at the beginning of the press cycle.

### **2.3.1 Conduction**

Conduction is thermal energy transfer from one body to another of different temperature by way of direct contact. This can occur between solids, fluids at rest or both, from the high thermal energy body to the low thermal energy body. Conduction is the means by which heat is transferred from the platens of the hot-press to the surface particles of the mat (Strickler 1959 and Bolton 1989). Conduction also occurs inside the mat, being most effective in the wood components, and less effective through the voids. Fourier's law describes this transfer of thermal energy based on a temperature gradient in the following equation (Siau 1995):

$$q = -k \frac{\Delta T}{\Delta x} \quad (4)$$

q = conductive heat flux in J/m<sup>2</sup>s

$\frac{\Delta T}{\Delta x}$  = temperature gradient

k = thermal conductivity in W/mK

Thermal conductivity in the longitudinal direction is approximately 2.5 times that in the transverse direction wood. This difference in conductivity is the direct result of cell wall

makeup and the alignment of the cellulose microfibrils with the longitudinal axis. Air has an extremely low thermal conductivity. This reduces the transverse thermal conductivity because of the air filled lumen spaces (Siau 1995, Kamke and Zylkowski 1989, Suleiman et al 1999).

There is a linearly increasing relationship in wood with thermal conductivity and density. This relationship exists in wood-based composites for densities below  $1000 \text{ kg/m}^3$ . Thermal conductivity is the highest for solid wood parallel to the grain and lowest for fiberboard, with wood-particle composites somewhere in between. Little work has been done to determine thermal conductivity parallel to the mat faces. Although some research by Humphrey (1982) and Ward and Skaar (1963) indicates that conduction parallel is approximately 50 percent higher than through the mat thickness.

Conduction plays a more important role in heat transfer as the mat is consolidated further and the void fraction in the mat decreases with increasing density. As this happens, air is removed from the mat, increasing the conductivity. Additionally, the face flakes are undergoing a densification process, which increases their individual conductivity. The consolidation process also increases interparticle contact, further increasing the conductivity.

### **2.3.2 Convection**

Convection is the transport of energy or mass by the movement of a fluid. This transport of energy or mass to and from (solid-solid or fluid-solid) surface interfaces is the result of molecular conduction and gross fluid movement. If the fluid movement results from

some external influence (fan, pump, wind) it is referred to as forced convection. During the hot-pressing of wood composites the steam produced from bound water in the wood particles and the water content of the resin is driven to the core. This process is more consistent with natural convection (Kay and Crawford 1993, Beiser 1973).

Early research conducted by Strickler (1959) indicated that convection is the primary means of heat transfer in the mat during wood-based composite manufacturing. This is also a later conclusion by Haas et al (1998), who stated that convection and hydrodynamic gas flow are the main heat and mass transport mechanisms. A review of the literature by Bolton and Humphrey (1988) also states that the majority of heat transfer in the case of particleboard is the result of convection.

Conduction, convection and gas flow are interdependent in the transfer of heat during hot-pressing. As the mat surface is heated the bound water in the strands closest to the hot platens is vaporized. This heating increases the vapor pressure near the surface strands early in the pressing operation. The core initially is still cold, creating a pressure differential from the surface layers to the core. This gradient now causes the heated water vapor to migrate to the core (Kamke and Wolcott 1991). As this vapor pressure boundary moves to the core, the temperature differential causes moisture to condense, thus liberating latent heat (Bolton, Humphrey and Kavvouras 1989a, Zombori 2001 and Strickler 1959). Previous research indicated that the gradient was caused only when the moisture in the furnish reached the boiling point. However the gradient requires only the change in temperature, thereby changing the equilibrium moisture content (Bolton,

Humphrey and Kavvouras 1989a). Shorter press closing times result in a faster build-up of vapor pressure in the surface flakes. This in turn produces a higher rate of convection to the core. Higher moisture content face layer flakes also contribute to faster temperature increases in the core by way of convection. Although these higher moisture content face flakes may negatively affect the maximum temperature achievable as compared to low moisture content pressing (Kamke and Casey 1988b).

The movement of heated water vapor to the core leads to a second pressure differential, which is oriented horizontally between the core (panel center) and the edges of the mat. This horizontal flow limits the total pressure achievable in the core during pressing and sometimes restricts the maximum core temperature reached (Kamke and Wolcott 1991).

If the vapor pressure migration to the edge is retarded, and the press opens prematurely, it is possible for the vapor pressure in the mat to cause delamination. With vapor pressure migration to the edge slowed to some degree, the core will increase in temperature much faster because of the pressurized steam effect. The reduction of edgewise cooling is an important concept in the manufacture of OSB panels; it allows for the more rapid heating of the core by convection (Kamke and Wolcott 1991).

## ***2.4 Permeability in Composite Pressing***

It is important in the discussion of permeability to define the directions of flow.

Throughout this literature review permeability through the panel thickness will be referred to as transverse permeability. Permeability in the plane of the panel will be referred to as in-plane permeability (See Figure 2-1).

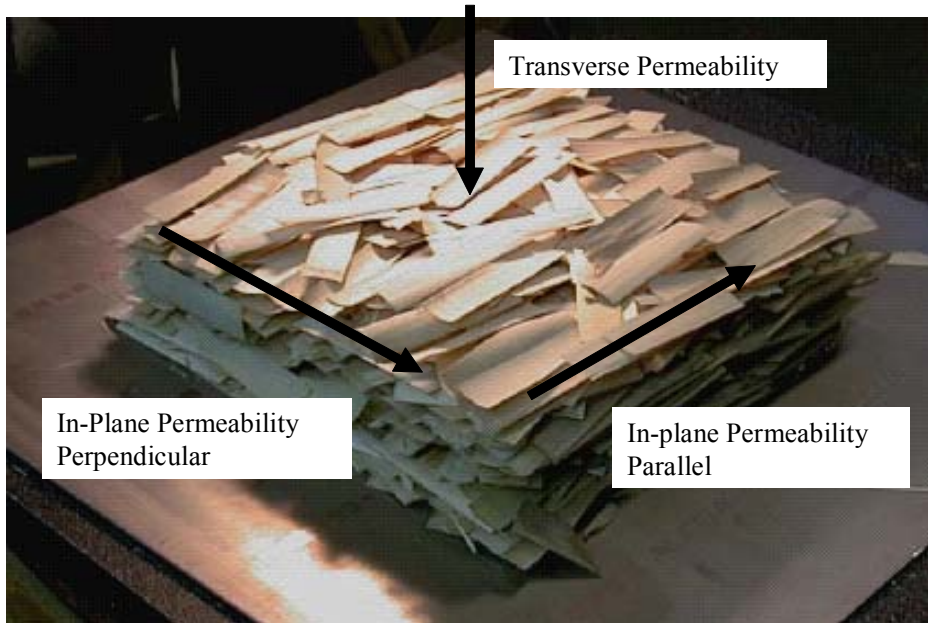


**Figure 2-1. The principal directions in OSB for permeability measurements.**

Results from Haas et al (1998) for fiberboard, particleboard and oriented strandboard clearly show that transverse permeability, and permeability parallel to the plane of the panel increases with decreasing density. The permeability values reached were based on finished panels of different densities and expressed in the following equation (see Table 2-1 for the coefficients):

$$K = \exp\left(\frac{1}{a + b\rho + c/\ln\rho}\right) \quad (5)$$

K = permeability

$\rho$  = density

a, b and c are coefficients

**Table 2-1. Transverse and in-plane permeability coefficients for equation 5.**

	Flow Direction	Resin Content (%)	a	b	c
von Haas et al. (1998)	Parallel				
	longitudinal	11	0.084	-7.26E-06	-0.746
	perpendicular	11	0.098	-9.78E-06	-0.819
	longitudinal	5	0.049	-3.22E-06	-0.540
	perpendicular	5	0.049	-2.41E-06	-0.540
	Transverse	11	-0.005	7.73E-06	-0.214
		5	0.043	-2.79E-06	-0.481

The method used in panel manufacturing reduced the potential vertical density gradient by consolidating the mats cold before applying heat for the cure. This allows for a permeability determination based on a constant density through the thickness. From this research permeability as a function of flake alignment was determined, with permeability being higher for flow parallel to the flake alignment. However, this study failed to address the changing density during the pressing operation and did not account for the horizontal variation in density.

No density was mentioned for the species used in the panel manufacturing so compaction ratio determination was impossible. However, through personal communication it was determined that *Pinus sylvestris* was the species used in the manufacture of the mats. Mats comprised of high-density species will have lower compaction ratios compared to low-density species. This will lead to mats with an increased number of voids and a potential increase in the number of pathways available for flow. It is therefore possible that two mats of the same density but comprised of different density species could have much different permeability characteristics. The flakes used were also much smaller than those employed in traditional OSB manufacturing.

Research conducted by D'Onofrio (1994) attempted to address the changes in permeability as it relates to changing density during the mat pressing operation. The mats analyzed in this research were 5 ½ inches in diameter and composed of aspen flakes. The flakes in this research were also much smaller than those in traditional OSB manufacturing, ranging in size 0.025 inches to 0.75 inches in width with 80% of those observed being under 0.5 inches in width. In this research heated platens were employed, so the influence of a vertical density gradient was present but not addressed. No research was conducted to determine how the change in density as the result of the consolidation process affected parallel permeability. Haselein's (1998) research employed a similar apparatus to D'Onofrio in determining permeability in the consolidation of fiberboard mats.

Research indicates that mats composed of larger flakes (like those found in OSB) have lower convective heat transfer rates to the core. These larger flakes also lead to mats with higher parallel permeability (Kamke and Casey 1998). The composition of an OSB mat results in polygonal pores for transverse flow, which are wider than they are long. Flow parallel to the panel plane encounters pores that are long wide slits between the flake faces. As a result, flow to the core encounters polygonal pores. Then the flow must negotiate large flakes affecting its pathway. This lengthens the path of travel for the gas molecules to the core compared to panels composed of smaller furnish. The difficulty of the pathway is generally referred to as tortuosity with panels composed of large flakes having a higher tortuosity factor (D'Onofrio 1994).

After densification, the polygonal pores are wider and shorter, less restricting to flow, while the slit type pores controlling parallel flow, show an increased resistance. With the panel's transverse permeability higher than that of longitudinal permeability in solid wood, it is obvious that the spaces between the flakes control the panel's permeability (Bolton and Humphrey 1994, Geimer 1975).

Density is directly related to available void spaces, and influences the tortuosity of the flow path. Fewer and smaller voids result in a lower permeability (Garcia 2002 and Geimer 1982). Bolton's (1989) model used data from Sokunbi (1978) for variation in permeability based on vertical density gradient. Some researchers showed that transverse permeability and the vertical density profile were a poor relationship, although there is clear evidence that an increase in panel density results in an increased likelihood for panel delamination due to excessive steam pressure (Bolton and Humphrey 1994).

During press closing the permeability is extremely high, because the void volume approaches 90 percent and these voids are connected via an extensive pathway system. During press closing the mat offers little resistance to vapor flow. Therefore, the maximum temperature rarely exceeds the boiling point of water (Kamke and Casey 1998). The heating of the core of the mat by convection is initially rapid. However, the core temperature is limited in the presence of sufficient water vapor due to the prevailing gas pressure. As the mat density increases permeability is reduced, gas pressure builds, and core temperature is able to rise. Mats formed with randomly aligned flakes have faster heating of the core do in part to their reduced parallel permeability (Garcia 2001).

Humphrey and Bolton (1989) proposed that the low-density core region controls permeability parallel to the panel surface. This is based on earlier research that indicated no changes in permeability parallel to the panel surfaces could be detected in panels over 15 mm thick. Smith (1982) reported waferboard permeability parallel increased with faster press closing times because of the lower core density. Humphrey and Bolton's (1989) work on extruded particleboard indicated that the ratio of parallel permeability to transverse was found to be approximately 59:1. Pichelin et al (2001) indicated that in high moisture content (over 20 percent) OSB pressing this ratio could reach as high as 100:1.

Bolton et al. (1989a) described pressing and curing of wood-based composites in a model based on five distinct periods. The press closing and the initial energy transfer from the hot platens to the mat characterize period A, as seen in Figure 2-2. Little if any temperature rise can be detected in the core, which indicates that insufficient energy has been transferred from the platens (Bolton et al. 1989a and Torrey 2001).

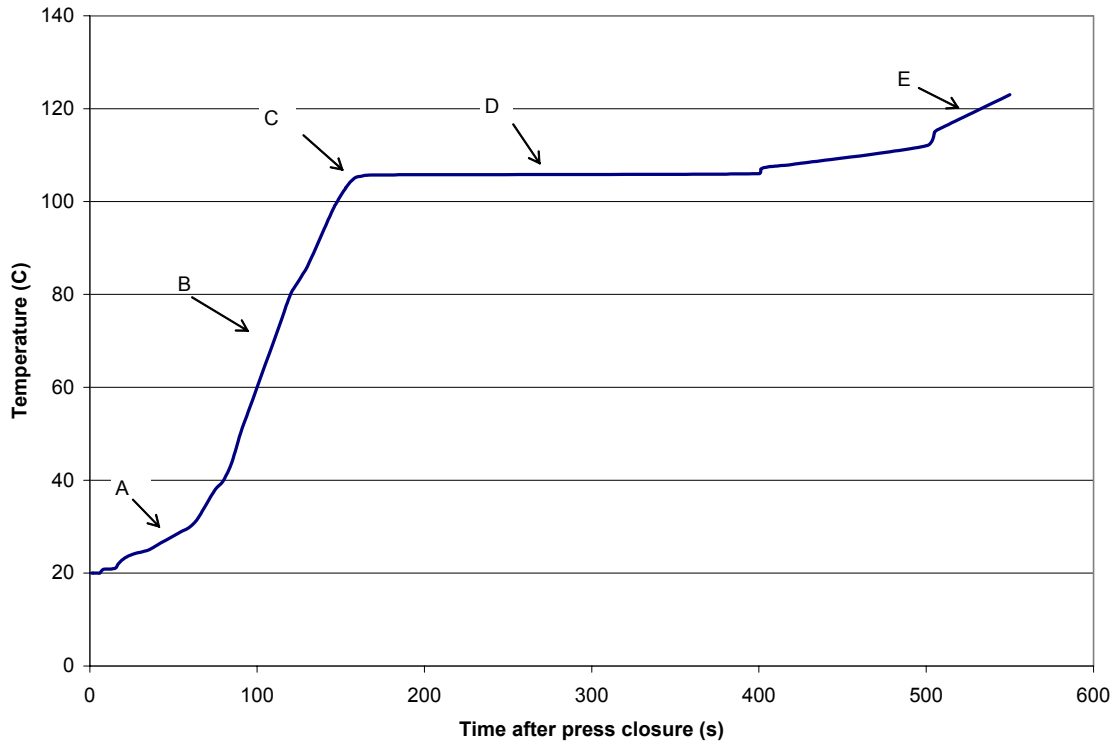


**Figure 2-2. Five period description of the mat core temperature change during the pressing operation (Bolton et al 1989a).**

Figure 2-3 shows the temperature gradient at different times during the press cycle. As the surface flakes warm an increase in the vapor pressure near the surface results. Figure 2-4 illustrates the changes in pressure at different stages in the press cycle. This gas pressure and temperature gradient encourages the flow of warm moist air to the core. A rapid rise in core temperature occurs as the moisture condenses, thus liberating the latent heat (Bolton et al. 1989a). Figure 2-5 illustrates the movement of moisture to the core based on the gas and temperature gradients during various stages of the press cycle.

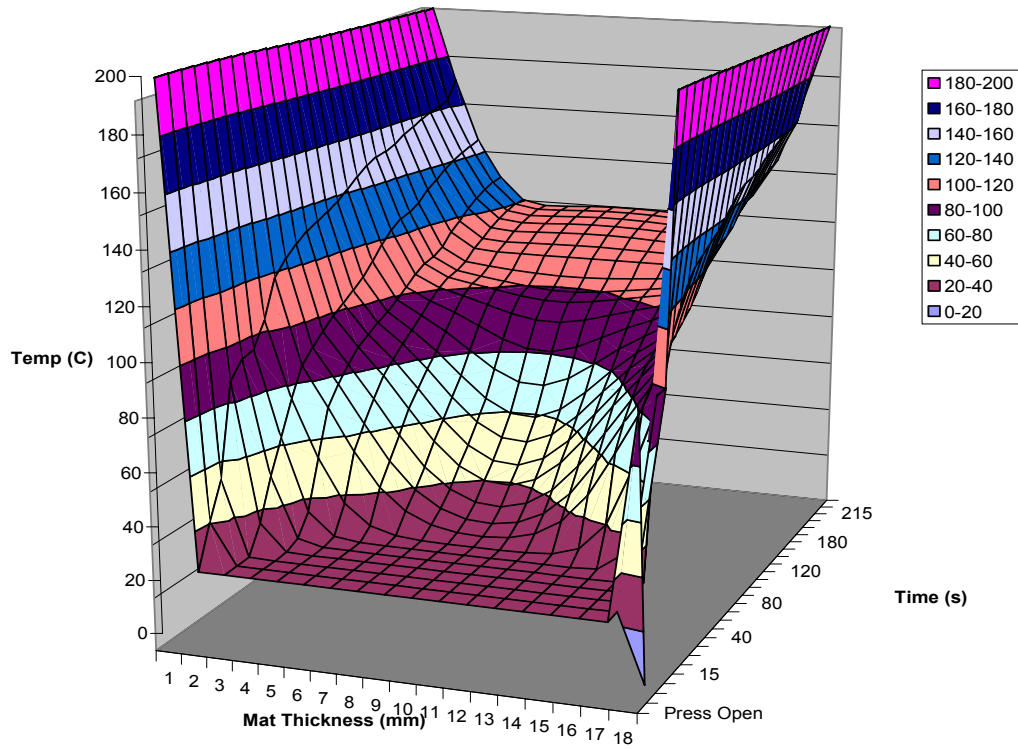


Figure 2-3. Temperature through the mat thickness at various times during the press cycle for an 18 mm thick mat.

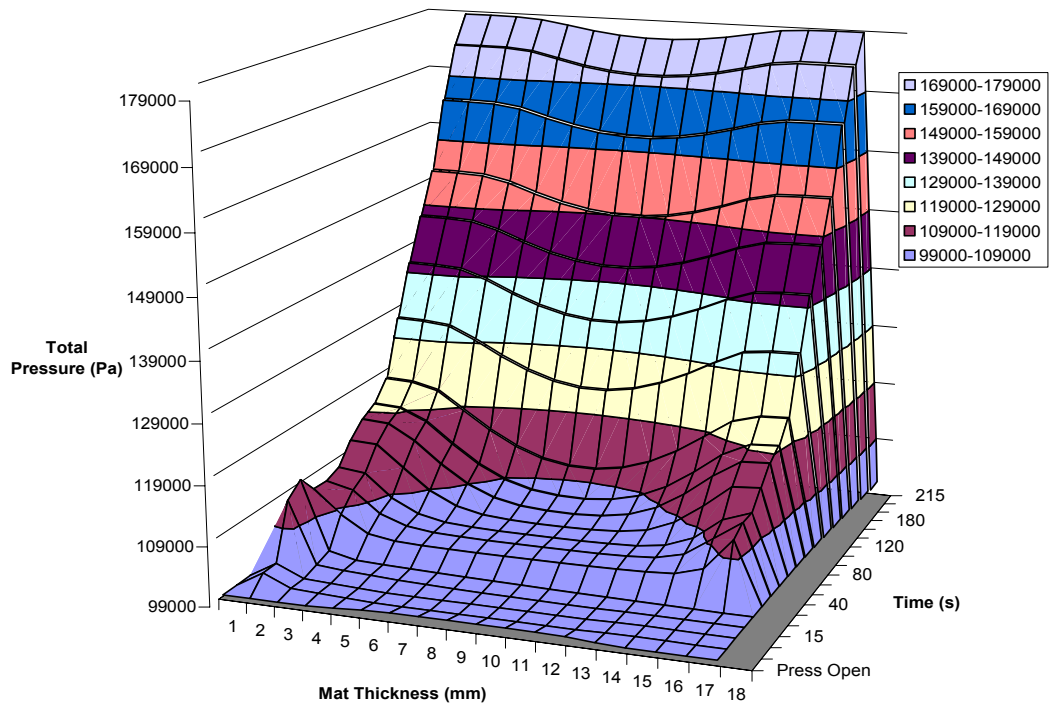
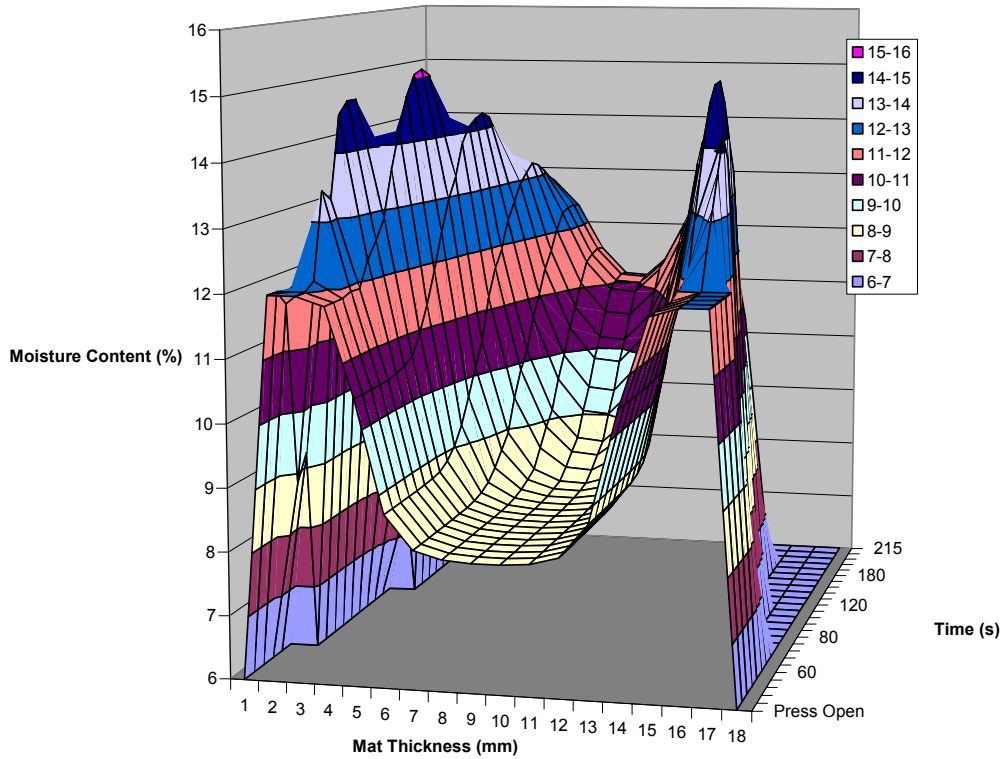


Figure 2-4. Total gas pressure at various stages during the press cycle for an 18 mm thick mat.



**Figure 2-5. Moisture content at various times in pressing based on an initial face flake moisture content of 12 percent and core flake moisture content of 8 percent for an 18 mm thick mat.**

Further, into the pressing operation the core temperature rise starts to slow, which indicates that the process has entered into period C. This period is classified by a mild temperature gradient. At this point during the process, less moisture is being evaporated from the surface flake layers, and therefore, less heated moisture is being forced to the core. As a result, the horizontal gradient driving heat and moisture through the mat edges causes the core to enter a near temperature and vapor pressure equilibrium (Bolton et al. 1989a).

Period D is characterized by a temperature plateau, which indicates there is no change in core temperature. Similar to period C any heat and moisture migration from the surface is equal to that lost through the edges (Bolton et al. 1989a).

Well into the pressing operation, a gradual increase in the core temperature characterizes period E. This is most likely the result of conduction, because most of the moisture has been driven from the surface flakes, although little value is provided by this period since it occurs too late in the press cycle (Bolton et al. 1989a).

This five period temperature profile changes somewhat when pressing mats with high moisture content furnish. Period B is broken into two phases, with the initial portion being a much slower temperature rise. The later portion is an extremely rapid, almost instantaneous, temperature rise. With the increase in moisture present in the core, period E can't be detected (Pichelin et al. 2001).

In Bolton's et al. (1989) five period description of the pressing operation, period B shows the importance of convection. During this period a rise of 80-100°C is the direct result of heat transfer by convection, accounting for approximately 75 percent of the temperature rise. Transverse permeability controls heat and moisture flow from the hot platens to the core. While permeability parallel controls flow from the panel center to the edges (Bolton and Humphrey 1994, Pichelin et al. 2001).

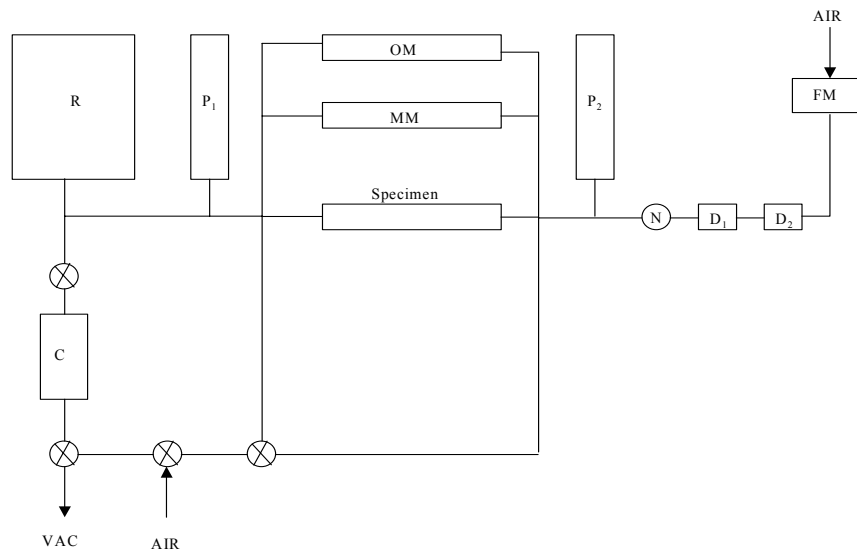
The same determination is supported by the results from high moisture content pressing conducted by Pichelin et al. (2001), where over 85 percent of the temperature rise is explained by convection. During high moisture content pressing, with fast press closing times, the heated vapor still flowed by convection, even through the high-density surface region in the mat. Further research revealed that high and low moisture content pressing, at a fast closing press time, resulted in a temperature rise of the same rate. This indicates that permeability is the controlling factor in heat transfer, not moisture content. At slower press closing times the vapor pressure gradient traces a path more to the edges of the board transporting less heat to the core. Comparing high and low moisture contents for long press closing times, moisture content was truly the deciding factor in the rate of core temperature rise (Pichelin et al. 2001).

Understanding and determining the permeability of wood composites during the hot-pressing operation will become increasingly valuable in the future. As more moisture tolerant adhesives are developed, a thorough understanding of heat and vapor flow will be required. Already it is recognized that higher moisture content pressing results in products with less residual stresses, thereby reducing thickness swell (Palardy et al. 1989).

## ***2.5 Methods of Measuring Permeability***

Various methods exist for determining the specific gas permeability of solid wood samples, which to a certain extent can be used in permeability determination for wood-based composites. Siau (1995) provides a schematic of an apparatus designed by Petty

and Preston (1969) that is easily adapted depending on accuracy required (Figure 2-6). This design employs a vacuum, which causes atmospheric pressure to force air through the specimen. In order for the apparatus in Figure 2-6 to be used for the determination of permeability in wood-based composites, a redesign of the specimen holder may be necessary.



R vacuum reservoir,  $P_1$  manometer,  $P_2$  manometer, C cartesian manostat, OM differential oil manometer, MM differential mercury manometer, N needle valve,  $D_{1\&2}$  dessicants, FM flowmeter.

**Figure 2-6. Apparatus for air permeability measurements (Siau 1995).**

This system allows for the determination of pressure drop over the length of the specimen by means of two pressure gauges. Depending on accuracy, it also allows for the

determination of pressure drop based on two differential manometers. The flow meter provides the remaining information necessary to determine specimen permeability.

Results from Haas et al (1998) were determined using an apparatus similar to Petty's, but compressed air was used to push air through the samples. D'Onofrio (1994) also employed a similar setup to Petty, but it differed in that the permeability readings were made on flakeboard mats during the pressing operation. The apparatus was connected to a fixture that allowed readings at various levels of mat consolidation.

Haselein (1998) employed a method that also allowed for measuring permeability during the consolidation process on fiberboard using compressed air as the test medium. In determining in-plane permeability holes were cut in the center of round fiberboard mats and the top and bottom faces were sealed. Gas was then injected into the hole and allowed to vent to atmosphere through the mat edges. A system of metal rings were employed during testing for transverse permeability, these compressed the mat edges preventing radial flow.

## ***2.6 Predicting Permeability in Other Porous Media***

The determination and prediction of permeability in porous media is extremely important in various industries. In the filtration of liquids and gasses, process efficiency is heavily dependent on an understanding of permeability. In the filtering of coal gas, dust particles buildup on filters resulting in a pressure loss. As more dust builds up the resulting filter cake undergoes compression from aerodynamic drag. This compression

reduces permeability further. To address this pressure loss, back pulses of pressure, where the flow is reversed, are periodically used to clean the dust cake from the filter (Neiva and Goldstein 2003).

Neiva and Goldstein (2003) conducted research in an effort to predict an optimal time for back pulse cleaning based on measured pressure loss. The following pressure loss equations were evaluated Carman-Kozeny, Happel's cell, and Darcy. The first two equations required that porosity, average particle diameter, and sphericity be known, while Darcy's does not. Modifying these equations based on volume of dust cake solids formed per time interval and specific cake resistance, lead to a pressure loss prediction based on time. The time predictions based on Darcy's law, Happel's cell and Carman-Kozeny differed 8 seconds, 5 minutes and 17 minutes respectfully from the actual, which corresponded to a relative error of 0.1, 3.3 and 10.6 percent.

Pressure loss predictions based on time using the Carman-Kozeny equation have their limitations based in the following. Kozeny theory explains permeability based on geometric properties of the porous medium. These properties consist of tortuosity, specific tube surface and the Kozeny constant. Of these, tortuosity is clearly an undefineable term in the equation. The Kozeny constant in early work by Kozeny is changed to fit the data after every experiment. Carman's modification of the equation introduces specific tube surface, which is the tube surface exposed to the fluid per unit volume of solid. The Kozeny constant is then held constant at a value of  $1/5$  (Scheidegger 1974).

Neiva and Goldstein (2003) applied the Carman-Kozeny equation by representing a dust filter cake as a pipe of some radius through which the fluid would flow. This required the defining of average particle diameter and particle sphericity, with a Kozeny constant assumed to be 5. The Happel's cell equation was applied by modeling incompressible fluid flow through the filter cake as a system of concentric spheres, with the internal sphere a solid and the outer sphere a frictionless fluid. Again this model required the defining of sphericity and particle diameter. As the above discussion shows the application of the Carman-Kozeny equation and the Happel's cell model to flow through wood particle composites would be problematic, with Darcy's law being the most applicable.

Fill time is an important factor in the manufacture of fiber-reinforced composites. During this process resin is injected into a mold containing a fiber or fabric preform. These preforms exist at various fiber volume fractions and alignments that affect permeability and contribute in some cases to anisotropy. Permeability is further effected by compression of the perform, which occurs when the mold is closed. Fill time predictions must be accurate enough so no dry spots exist after filling and the process is completed efficiently. Manipulation of Darcy's law incorporating preform porosity can accurately predict fill time in many fiber reinforced composites with randomly aligned fibers being the most accurate (Gardner 2002).

### **3 Materials and Methods**

This chapter details the approached to the experimental work conducted. Four sections describe sample preparation and design, sample test methods, commercial mat comparisons and the statistical methods employed for data analysis. For the remainder of this thesis the permeability referred to is superficial gas permeability, as defined earlier in Equation 2.

#### **3.1 Sample Preparation**

Oriented strandboard (OSB) mat permeability measurements were conducted on both in-plane permeability and transverse permeability (permeability through the mat thickness) specimens.

##### **3.1.1 Flake Preparation**

OSB mats for determining in-plane permeability were prepared from yellow-poplar (*Liriodendron tulipifera*) flakes cut on a laboratory disk flaker and dried in a kiln to approximately 2-4 percent moisture content. The flake length was 4-inches and the width 1-inch. Since the flakes were cut from blocks, with a thickness of 1-inch and a length of 4-inches, the flake dimensions were very uniform. Permeability measurements were made on mats at various compaction ratios (target mat density/raw material density). These compaction ratios are based on target mat density. The species density (ovendry basis) was restricted to the range of  $433\text{kg/m}^3 \pm 16 \text{ kg/m}^3$ . This density restriction was chosen based on the raw material available for flake manufacturing for this study and the desire to closely control compaction ratio. The target moisture content of the flakes was

typical for a commercial process. Once dried, the flakes were stored in plastic bags to retard any moisture gain or loss, as were the finished samples. By the time the permeability tests were conducted the flakes and finished samples were at a moisture content between 6 and 7 percent.

### 3.1.2 In-Plane Permeability

In-plane permeability measurements were made on mats comprised of flakes of the same thickness. The flake thicknesses examined were 0.05, 0.076, and 0.10-cm. The experimental design consisted of five compaction ratios (target panel density/raw material density) for mats prepared with 0.076 cm thick flakes.

**Table 3-1. Mat densities, flake thickness and number of samples for in-plane permeability determination.**

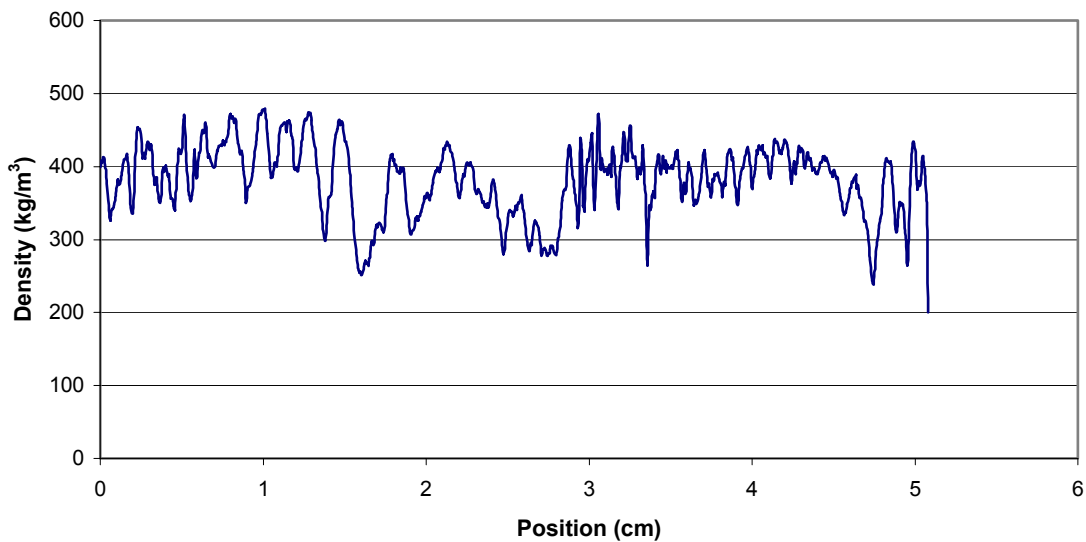
Density (kg/m <sup>3</sup> )	Compaction Ratio	Number of Samples/Flake Thickness		
		0.05 (cm)	0.076 (cm)	0.10 (cm)
120	0.28		5	
400	0.93		5	
560	1.30	5	5	5
640	1.48		5	
800	1.85		5	

Table 3-1 shows mat target density for a given number of samples at various flake thicknesses. This density range was designed so that permeability measurements from the sample mats would be in the range of commonly manufactured OSB. The measurements at densities of 120 and 400 kg/m<sup>3</sup> make permeability determination possible for densities that would be encountered initially in the pressing process. This range then reflects how permeability would change as a mat is consolidated. For the

compaction ratio corresponding to the 560 kg/m<sup>3</sup> mats, two additional treatments were applied, consisting of five mats prepared with flakes 0.05-cm thick and five prepared with 0.10-cm thick flakes. The difficulty involved in sample preparation and data collection dictated this reduced comparison. However it was still possible to determine from this design what influence flake thickness has on in-plane permeability. All 35 mats had permeability determined, in the flake alignment direction (in-plane parallel) and across the flake alignment direction (in-plane perpendicular).

The mats were 5 cm thick, 28 cm wide and 28 cm long. Mats were formed without resin in a stackable forming box using a laboratory flake aligner. Flake alignment was achieved using a series of vibrating parallel metal plates that only allow the flakes to fall on the mat being formed once they have achieved a constant orientation. Once the 400, 560 and 640 kg/m<sup>3</sup> mats were formed, they were cold pressed in a laboratory press between two cauls to a thickness of 3.5 cm. The lack of heat in the pressing operation resulted in the formation of mats with no vertical density gradient, so the corresponding permeability measurements were based on a constant density through the thickness (see Figures 3-1 and 3-2). The vertical density profiles were determined using a QMS density profiler. Formations of vertical density gradients require elevated temperatures and moisture to plasticize the wood flakes. Flakes near the hot platens soften because of their reduced compressive strength and densify more readily than those in the cooler core, resulting in a mat with high-density faces and a low-density core. If the temperature and moisture content are constant throughout the mat thickness, then no vertical density gradient will result (Kelly 1977 and Suchsland 1962). The 120 kg/m<sup>3</sup> mats did not

require the laboratory press. They were pressed by hand to stops for the corresponding density. The 800 kg/m<sup>3</sup> mats required steam-injection hot-pressing and a resin content of 3% per dry weight, again resulting in a mat with little vertical density gradient (see Figure 3-3). By introducing steam early in the compression stages of hot-pressing (at specific gravities below 0.27) the mat core temperature increases rapidly. In some studies the core temperature increased to 104° C in a matter of seconds after the introduction of steam. This rapid core temperature rise effectively results in a mat with a constant temperature and moisture content through the thickness, resulting in a reduced vertical density gradient (Geimer et al. 1992 and Geimer and Kwon 1999). These high density mats required more restraining force than possible with the sample design therefore requiring a finished panel to make testing possible.



**Figure 3-1. Vertical density profile for 400-kg/m<sup>3</sup> mat.**

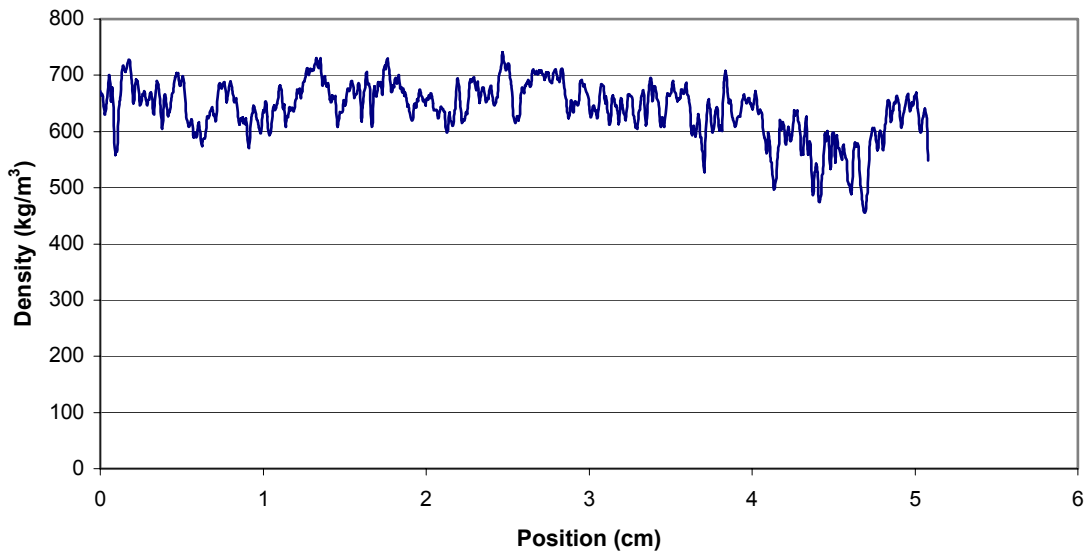


**Figure 3-2. Vertical density profile for 640-kg/m<sup>3</sup> mat.**

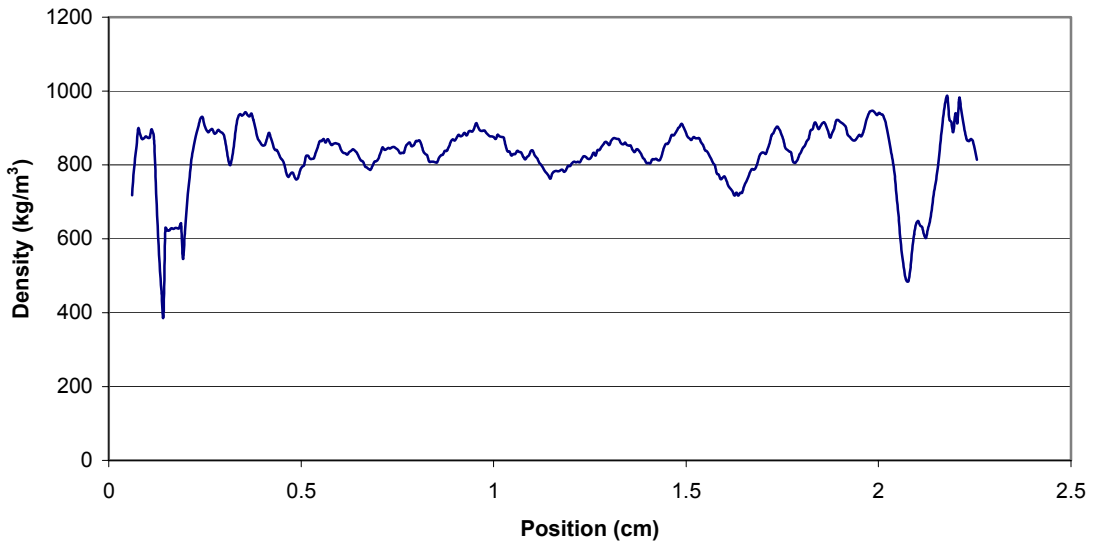


**Figure 3-3. Vertical density profile for 800-kg/m<sup>3</sup> mat.**

Once the mats were formed and pressed, they were transferred from the cauls and sandwiched between two ¾ inch plywood squares, where the mats were allowed to

recover to a thickness of 5-cm. They were restrained from further recovery by placing 2 wood screws 3.5-inches in length through the top and bottom plywood square. The resulting plywood and mat combination was then trimmed on a band saw to the desired dimension (see Figure 3-4).



**Figure 3-4. OSB sample mat restrained by plywood.**

Once trimmed to desired dimensions, silicone sealer was applied to 2 sides opposite each other and covered by  $\frac{1}{4}$ -inch plywood, which was held in place by wood screws. The wood screws through the thickness were then removed and the  $\frac{1}{4}$ -inch plywood and the screws on the side now restrained the mat.

The application of silicone restricts the airflow to the mat and does not allow the flow to bypass the mat and trace the plywood sides. The viscosity of the silicone sealant prevents any deep penetration into the mats, which could obstruct voids or pathways for flow. The silicone and plywood was first applied to test in-plane permeability parallel. Then the plywood was removed, and the mats were trimmed on the band saw to remove the

silicone. The silicone and plywood were reapplied to the remaining sides and in-plane permeability perpendicular was then tested.

To improve the seal on the supply and exit side of the samples a ridge of silicone was applied, which behaved as a gasket between the mat and the specimen holder and prevented air leakage. Figure 3-5 shows finished in-plane permeability samples. Screens were employed on the supply and exit side of the sample holder to provide a better distribution of airflow. This method kept the supply and exit lines from becoming blocked. The size of the samples and the corresponding areas created large forces that could deflect the plywood enough to create air leaks when under pressure. Figure 3-6 illustrates the manner in which the sample was restrained from deflection and the means by which decompression at higher gas pressures was prevented. The sample top and bottom were restrained by placing the entire holder in a small laboratory press to prevent expansion.



**Figure 3-5. In-plane permeability specimens at all five density levels increasing from left to right.**



**Figure 3-6. In-plane permeability specimen holder.**

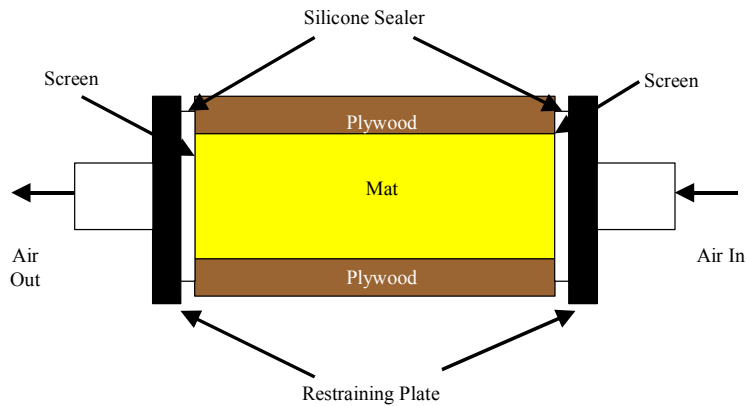


**Figure 3-7. Cut away view of in-plane permeability specimen.**

### **3.1.3 Transverse Permeability**

The experimental design consisted of six compaction ratios for mats formed with 0.076 cm flakes, while mats formed with 0.05 and 0.1 cm flakes were subjected to only 5 compaction ratios.

**Table 3-2 . Panel densities and the corresponding number of samples per flake thickness.**

Density (kg/m <sup>3</sup> )	Compaction Ratio	Number of Samples/Flake Thickness		
		0.051 (cm)	0.076 (cm)	0.102 (cm)
120	0.28	5	5	5
300	0.70	5	5	5
400	0.93	5	5	5
560	1.30	5	5	5
640	1.48	5	5	5
800	1.85		5	

For transverse permeability measurements an apparatus was designed to allow the forming of a flake aligned mat and its compression in a laboratory press (see Figures 3-8 through 3-10). The flake alignment was achieved using a series of vibrating parallel metal plates that only allow the flakes to fall on the mat being formed once they have achieved a constant orientation. The mat target densities of 120-640 kg/m<sup>3</sup> shown in Table 3-2 are based on a final density of 800 kg/m<sup>3</sup> at a thickness of 0.95 cm. For each sample the target density was achieved by closing the press to a particular opening. Only one mat was required for all five-density observations 120-640 kg/m<sup>3</sup>. The 800 kg/m<sup>3</sup> samples were 2.54 cm thick steam-injected panels tested in the before mentioned apparatus. This departure from the previously mentioned sample design was necessary due to the force requirements for cold pressing a mat to 800 kg/m<sup>3</sup>, which was not possible with the apparatus design nor the laboratory press. By cold pressing the 120-640 kg/m<sup>3</sup> mats and steam-injection pressing the 800 kg/m<sup>3</sup>, mats permeability measurements were made on mats with no vertical density gradient or at least greatly reduced gradients, allowing for a direct density versus permeability comparison.



**Figure 3-8. Transverse permeability specimen holder.**

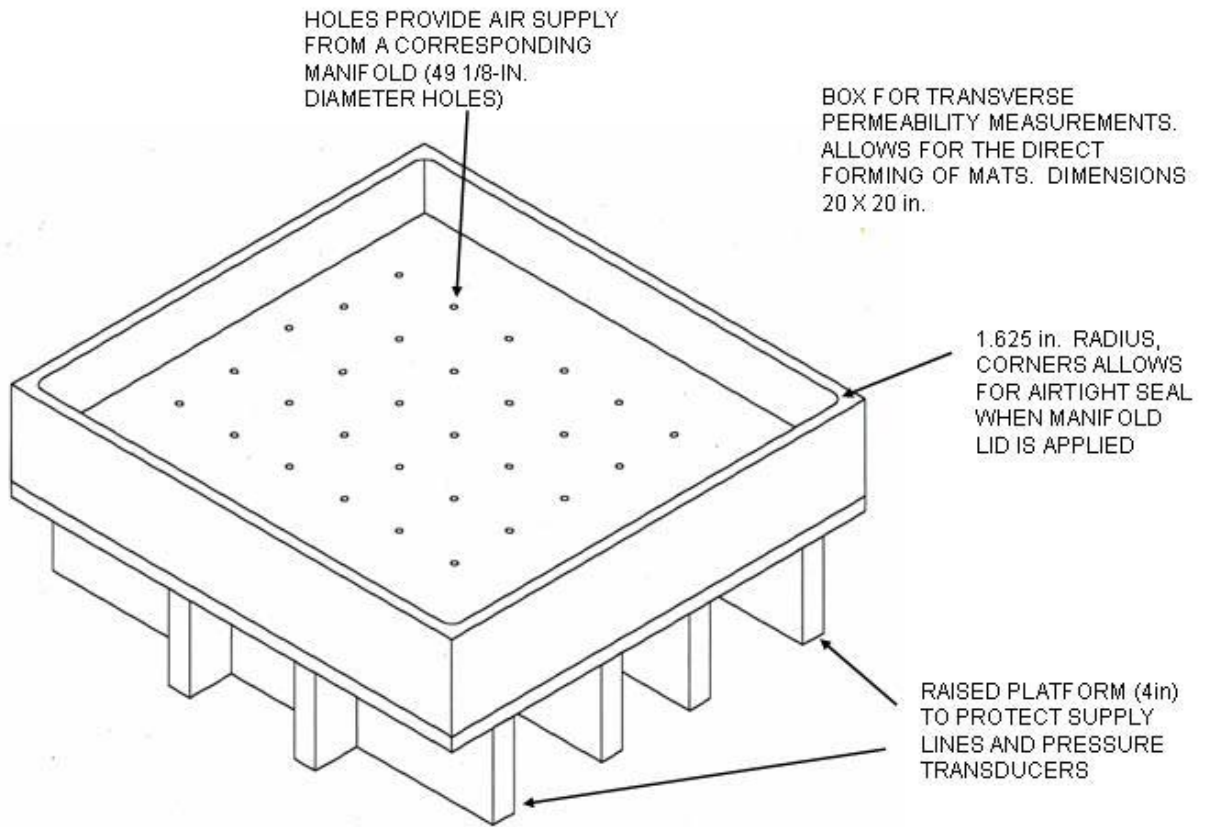


**Figure 3-9. Detailed description of the transverse permeability box.**

THE LID WAS DESIGNED TO COMPACT OSB MATS TO A DESIRED DENSITY. THIS LID GOES INSIDE THE BOX DESCRIBED IN THE PREVIOUS FIGURE. ANOTHER RAISED PLATFORM IS THEN PLACED ON THE LID TO PROTECT THE EXIT LINES AND ALLOW FOR THE PRESSING OF THE LID INTO THE BOX.

HOLES RECEIVE AIR AFTER IT PASSES THROUGH THE MAT (49 1/8-in DIAMETER HOLES) A MANIFOLD THEN DIRECTS THE AIR TO AN EXIT LINE WHERE A PRESSURE TRANSDUCER AND FLOWMETER RECORD DATA.

28 COUNTERSUNK MACHINE SCREWS ATTACH AN 1/8-in. THICK ALUMINUM PLATE TO A 1-in. THICK ALUMINUM PLATE TO CREATE THE MANIFOLD.

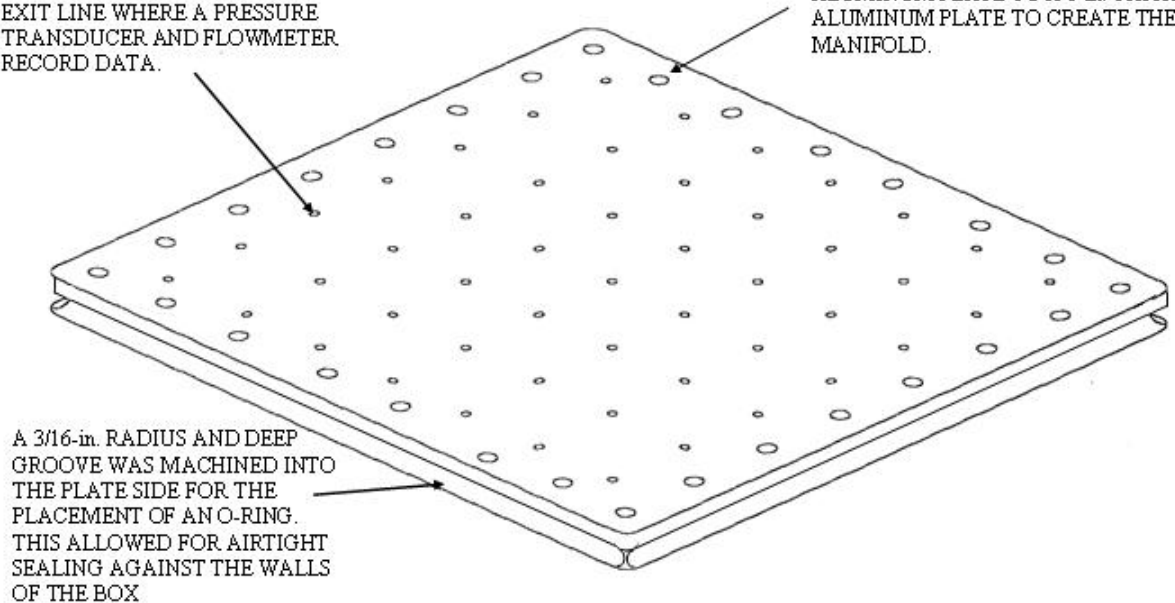


Figure 3-10. Detailed description for the transverse permeability box lid.

### 3.2 Experimental design

In this experiment OSB mat permeability was the desired response variable to be measured. Several factors were identified that could potentially influence the response and are listed as follows. Heated platens used in the consolidation process could result in a mat with a vertical density gradient further complicating the detection of a permeability density relationship. Species density influences the resulting compaction ratio.

Variability across flake moisture content could lead to localize areas of increased flake

plasticization, thus increasing the potential for horizontal density variation. The sample preparation and design mentioned in the previous section were used to reduce or eliminate any of these potential factors influence on the response. This design was used to limit the variability in OSB mat permeability directly to flake thickness and compaction ratio.

The experimental design shown in Table 3-1 and 3-2 is consistent with a fractional factorial experiment. This approach reduces the number of samples required to determine how flake thickness influences permeability. In both the transverse and in-plane permeability experiments the mats comprised of 0.076-cm thick flakes serve as a treatment control to compare the effects of flake thickness. In the transverse permeability comparisons, only the 1.85 compaction ratio is limited to the 0.076-cm thick flakes. In the case of in-plane permeability, the flake thickness influence was only investigated for the compaction ratio of 1.3. It must be assumed then that any relationship existing at this compaction ratio is the same for all compaction ratios.

### **3.3 Apparatus**

Transverse and in-plane permeability was determined using the same apparatus, similar to that described by Siau (1995), with only a modification to the specimen holder. Three flowmeters, with ranges of 0.003-.08, 0-0.28, and 0-1.27 m<sup>3</sup>/min were used. At high compaction ratios the flow rates are greatly reduced. Therefore flowmeters with a narrower range were necessary to determine flow accurately. Two pressure transducers were employed one on the high-pressure side of the specimen and one on the low-pressure side. These were used to determine the pressure differential across the

specimen, average pressure and the pressure at the flow measurement location. Figure 3-11 provides a schematic of the apparatus.

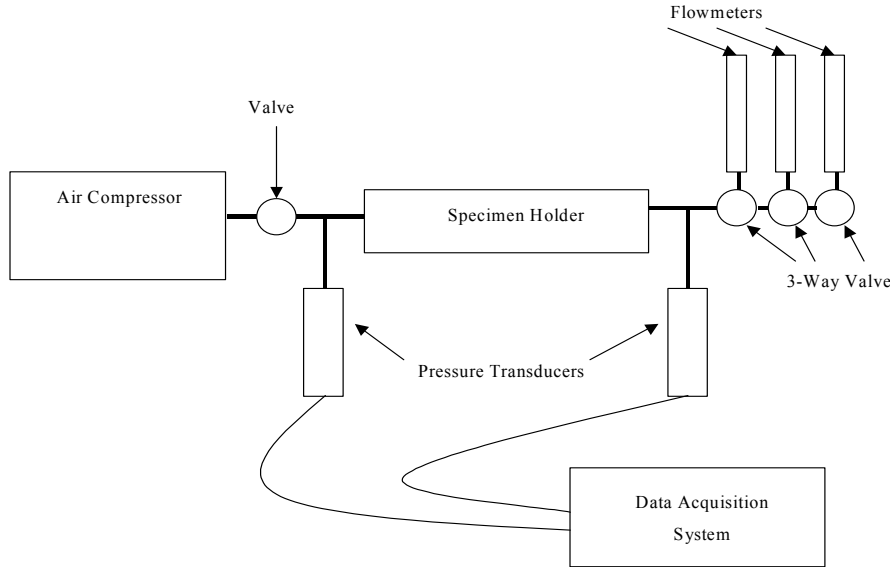


**Figure 3-11. Apparatus design for permeability measurements in OSB mats.**

The flowmeters were manually operated and required the manual recording of results.

The pressure transducers provided a voltage output signal that was recorded by a data acquisition system in a corresponding 0-140 kPa scale with an accuracy of  $\pm 200$  Pa.

At each compaction ratio, for transverse and in-plane permeability, sample permeability determinations were made at 5 distinct pressure differentials. A value was not recorded until the system achieved steady state. The pressure differentials coincided with the supply side pressures of 35, 48, 69, 83 and 103 kPa for each sample. From this it could be determined whether or not the samples deviated from the assumption of laminar flow.

To detect leaks, a soap-water solution was applied to every fitting employed in the apparatus. If leaks were detected the fitting was tightened and eliminated. For the

specimen holders used for transverse permeability and in-plane permeability the same solution was applied to the external areas, if leaks were detected then the samples were resealed.

### **3.4 Commercial Mat Comparisons**

To understand how OSB mats from commercial facilities may differ from that of OSB mats made from the laboratory flakes in this study, in-plane permeability and transverse permeability samples were prepared using commercial flakes obtained from a Weyerhaeuser facility in Elkin, North Carolina. These flakes were a mixture of various softwood species. In-plane permeability measurements were conducted on samples of the same design described in section 3.1.2 and transverse permeability measurements were made in the same manner as described in section 3.1.3.

Tables 3-3 and 3-4 show target densities for the commercial flake mats. High density mats ( $> 560 \text{ kg/m}^3$ ) were not included because initial statistical testing indicated little change in permeability could be detected above the density of  $560 \text{ kg/m}^3$  in the laboratory mats.

**Table 3-3. Mat densities for in-plane permeability samples for commercial flake mats.**

Density ( $\text{kg/m}^3$ )	Number of Samples From Commercial Fakes		
120		2	
400		2	
560		2	

**Table 3-4. Mat densities for transverse permeability samples for commercial flake mats.**

Density (kg/m <sup>3</sup> )	Number of Samples From Commercial Fakes		
120		2	
300		2	
400		2	
560		2	

For comparison with the laboratory flakes, it was necessary to determine the density and geometry of the commercially produced flakes. A sample of commercial flakes was obtained that corresponded to the weight required to form the highest density mat (3,780 g). This sample was then separated into five size classifications using a series of sifting screens. A total of 500 flakes were selected from this sample. The amount selected from each classification was based on a percent of total weight. For example, size classification 1 had 48 flakes selected based on the fact it made up 9.6 percent of the total weight. This was done in an effort to address the effect of flake size on permeability in the commercial mats. For each flake size classification, the weight was determined for each flake using a balance accurate to 0.01 g. The thickness was determined for each flake using a caliper accurate to 0.1 mm. These flakes were then scanned with a flatbed scanner to obtain a digital image of flake shape. Image analysis software (Image Pro, Media Cybernetics) was used to determine the apparent length and width of each flake (Zombori 2001). The apparent flake length and width were defined by a function of the flake's projected area and perimeter. The following equations describe how the apparent length and width were determined.

$$l = (P + \sqrt{P^2 - 16A}) / 4 \quad (6)$$

$$w = (P - \sqrt{P^2 - 16A}) / 4 \quad (7)$$

$l$  = apparent length (cm),

$w$  = apparent width (cm),

$P$  = perimeter of the flake (cm),

$A$  = area of the flake (cm<sup>2</sup>).

From the flake area, thickness and weight data, the individual flake density could be determined. This allows for the determination of the commercial mat compaction ratio, so a direct comparison between experimental mats and those made of commercial flakes is possible.

### **3.5 Data Analysis**

An Excel spreadsheet was used to calculate permeability based on the data acquired and all statistics were generated with SAS (statistical analysis software). Analysis of variance was employed to test for significant differences in target compaction ratios within flake thickness classifications and across thickness classifications for transverse and in-plane permeability. A 95 percent confidence level was used. Further tests for significance employed Tukey's honestly significantly difference test ( $\alpha = 0.05$ ).

With a desired objective being an empirical equation that predicts permeability based on compaction ratio and flake thickness, stepwise multiple-regression analysis was performed to determine which variables could be included in the model. Stepwise regression starts with no variables in the model and first adds the most significant. It will

then add another variable, and could possibly remove it, if it is not significant.

Stepwise regression will continue until no significant variable is left out of the model and no insignificant variable is left in the model. The determination of significance is based on an alpha value of 0.05.

For analysis of variance conducted on transverse permeability values from a single mat, it is assumed that the results for each compaction ratio are independent. This is not necessarily true statistically speaking, because the permeability results for each compaction ratio were determined on the same mat. The assumption for independence is based in the belief that the changes the mat undergoes between each compaction ratio (i.e. compression of the mat from a low density entity to a high density for the various compaction ratios) changes the structure so much that at each compaction ratio it is an entirely different structure. Without this assumption, analysis of variance within each flake thickness is not possible. However this question of independence has no bearing on the validity of comparisons across flake thicknesses. Analysis of variance conducted on the results from in-plane permeability is completely valid, because a separate mat was made for each compaction ratio.

## **4 Results and Discussion**

This chapter is divided into four sections detailing the results from the transverse and in-plane permeability experimental work, as well as the results from the commercial flake comparison. It also includes comparisons to previous work conduct by Haas (2000).

### ***4.1 Transverse Permeability Results***

Transverse permeability measurements were conducted on five separate mats at various compaction ratios for three different flake thicknesses. This permeability calculation was based on Equation 2 for superficial permeability. For each mat, five sub-samplings were conducted based on different pressure differentials.

OSB mats comprised of 0.05-cm thick flakes exhibit decreasing permeability as compaction ratio increases. Reductions in permeability are initially steep with increasing compaction ratios, but beyond the compaction ratio of 0.93, the reduction in permeability is less severe. It is clear in Figure 4-1 that the relationship between permeability and compaction ratio is non-linear. Analysis of variance conducted based on sub-sampling reveals a significant difference in permeability measured at each compaction ratio ( $p < 0.005$ ). Further comparisons with Tukey's honestly significant difference (HSD) test reveals, that permeability for the compaction ratios of 1.3 and 1.48 is not significantly different.

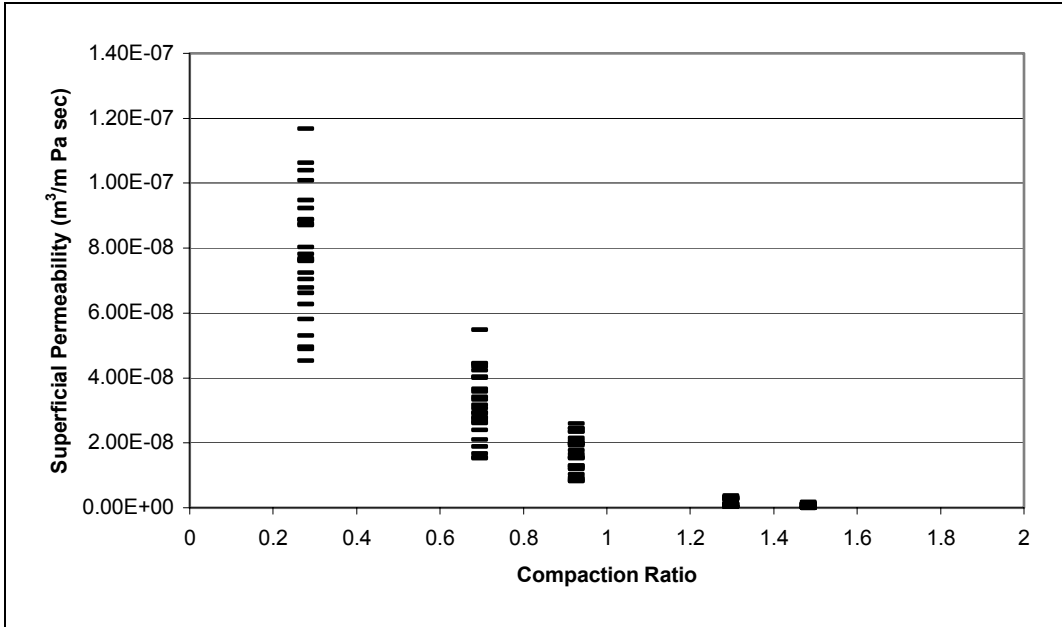


**Figure 4-1. Superficial permeability versus compaction ratio for OSB mats comprised of 0.05 cm thick flakes. Each compaction ratio shows results from all five mats as well as the five sub-measurements.**

Permeability measurements conducted on mats comprised of 0.076 cm thick flakes included measurements at an additional compaction ratio (see Figure 4-2). Again for OSB mats comprised of 0.076-cm thick flakes the relationship between permeability and compaction ratio appears non-linear. As the compaction ratio increases, observed permeability decreases. Beyond the compaction ratio of 1.3 reductions in permeability become less severe. Analysis of variance reveals that permeability at each compaction ratio is significantly different ( $p < 0.001$ ), with Tukey's HSD indicating that the resulting permeability for compaction ratios 1.3-1.85 is not significantly different.

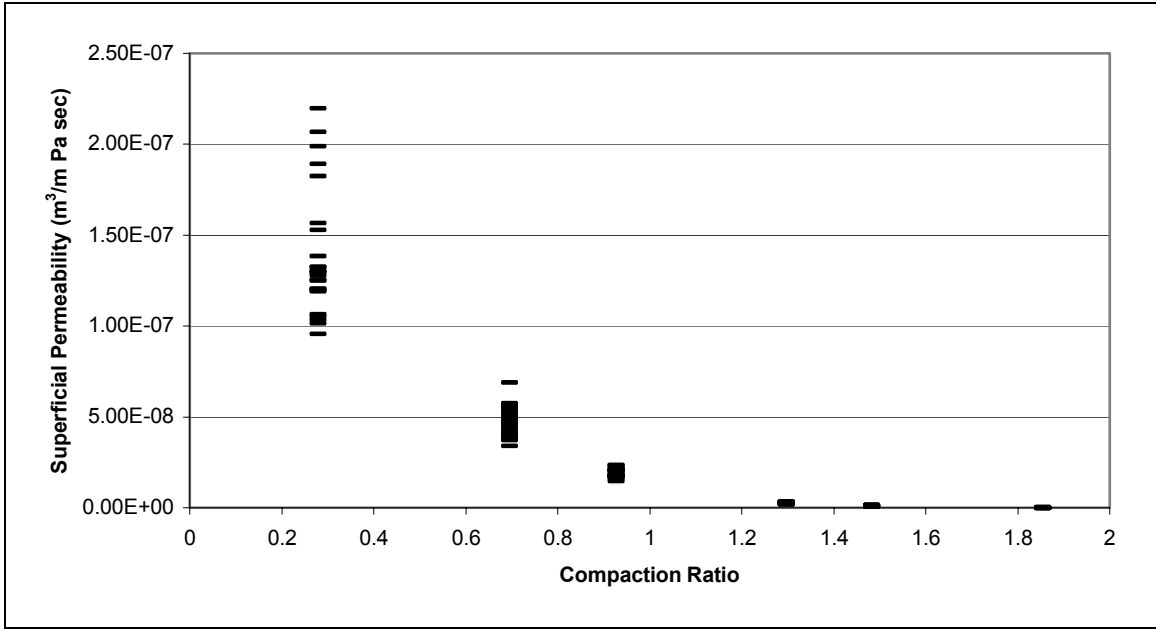


**Figure 4-2. Superficial permeability versus compaction ratio for OSB mats comprised of 0.076 cm thick flakes. Each compaction ratio shows results from all five mats as well as the five sub-measurements.**

OSB mats comprised of 0.10-cm thick flakes exhibit a decrease in permeability with increasing compaction ratios along with a high degree of variability until the compaction ratio reaches 1.3 (Figure 4-3). Analysis of variance fails to detect any significant difference in permeability for each compaction ratio, but Tukey's HSD indicates that 1.3 and 1.48 are the only compaction ratios that are not significantly different.

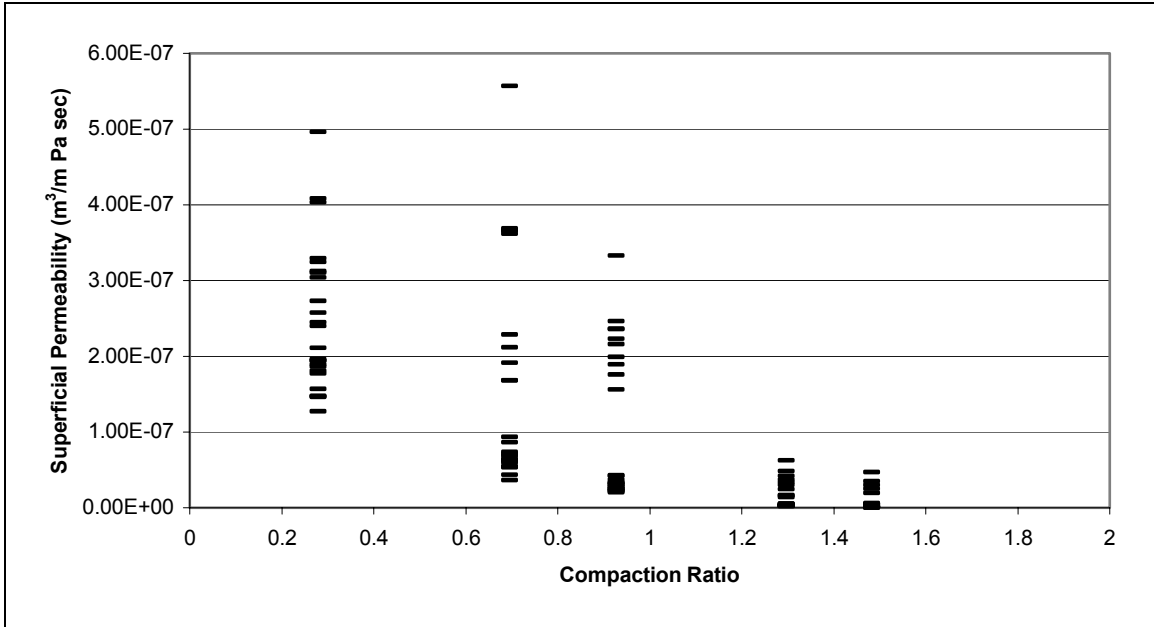


**Figure 4-3. Superficial permeability versus compaction ratio for OSB mats comprised of 0.10 cm thick flakes. Each compaction ratio shows results from all five mats as well as the five sub-measurements.**

Tables 4-1 to 4-3 provides transverse permeability summary statistics for all mats tested.

The coefficient of variation indicates that the highest variability in permeability is encountered at the highest compaction ratios. For a mat to be permeable, pathways through the thickness must be available to connect the existing voids. At low compaction ratios this connectivity between the voids is nearly a 100 percent. As compaction ratio increases, the connectivity of the voids is reduced. At this point any non-uniformity in mat forming has a critical impact on the permeability determined. Hence, the variability in permeability is increased with increasing compaction ratio. In no case even at the highest compaction ratios, was the permeability ever zero, indicating that the mats always remained permeable.

**Table 4-1. Superficial permeability (m<sup>3</sup>/m Pa sec) for mats comprised of 0.05-cm thick flakes.**

Compaction Ratio	0.28	0.69	0.93	1.3	1.48
Mean	7.80E-08	3.17E-08	1.68E-08	1.67E-09	6.46E-10
Standard Deviation	1.90E-08	1.02E-08	5.57E-09	1.24E-09	5.48E-10
Minimum	4.54E-08	1.53E-08	8.21E-09	3.59E-10	5.60E-11
Maximum	1.17E-07	5.49E-08	2.60E-08	3.82E-09	1.80E-09
cov%	24.42	32.36	33.19	74.21	84.83

**Table 4-2. Superficial permeability (m<sup>3</sup>/m Pa sec) for mats comprised of 0.076-cm thick flakes.**

Compaction Ratio	0.28	0.69	0.93	1.3	1.48	1.85
Mean	1.39E-07	4.76E-08	1.92E-08	2.67E-09	1.08E-09	4.75E-11
Standard Deviation	3.46E-08	7.75E-09	2.42E-09	4.31E-10	2.6E-10	9E-11
Minimum	9.58E-08	3.39E-08	1.46E-08	1.92E-09	6.71E-10	8.12E-13
Maximum	2.2E-07	6.88E-08	2.35E-08	3.39E-09	1.5E-09	3.41E-10
cov%	24.88	16.29	12.56	16.17	23.97	189.62

**Table 4-3. Superficial permeability (m<sup>3</sup>/m Pa sec) for mats comprised of 0.10-cm thick flakes.**

Compaction Ratio	0.28	0.69	0.93	1.3	1.48
Mean	2.47E-07	1.57E-07	1.06E-07	1.53E-08	8.18E-09
Standard Deviation	9.48E-08	1.41E-07	1E-07	1.75E-08	1.27E-08
Minimum	1.28E-07	3.66E-08	2.08E-08	2E-09	7.42E-10
Maximum	4.97E-07	5.57E-07	3.33E-07	6.29E-08	4.74E-08
cov %	38.47	89.68	94.33	114.35	155.76

As the compaction ratio is increased, the available pathways for flow are reduced. At a compaction ratio of 1.3 and beyond no statistically significant difference in permeability can be determined. Mats comprised of thicker flakes had higher permeability. This is the result of fewer flakes being required to form a mat of the same density. By reducing the number of flakes required to make the mat, the tortuosity of the flow path is reduced, therefore increasing the permeability. If the number of flakes required to make the mat is increased, then the flow occurring must negotiate an increased number of flakes increasing the tortuosity of the flow pathway.

As the mats are further compressed to higher compaction ratios, the pathways available for flow are reduced and many are eliminated, thus lowering the permeability. In the thinnest flake mats investigated, this reduction in permeability is initially abrupt. In the mats comprised of 0.10-cm thick flakes, the reduction in permeability does not occur in the same manner. This likely results from the decreased number of flakes required to form the mat as well as the influence mat forming could possibly have on the permeability. With fewer flakes involved in the forming of the mat, the placement of each flake is critical and potentially has the ability to drastically influence permeability. The thicker flakes are also less pliable under compression so the chance for damage to the flakes is greater. This damage could therefore increase the number of pathways available for flow or lead to a less abrupt reduction in permeability. This flake damage theory was proposed by D'Onofrio (1994) after a similar phenomenon was encountered at low moisture content pressing.

Further analysis across flake thickness reveals that permeability increases for increasing flake thickness. For permeability determined at a compaction ratio of 0.28 all flake thickness resulted in significantly different permeability based on analysis of variance ( $p < 0.0001$ ) and Tukey's HSD. However, at compaction ratios higher than 0.28 no significant difference in permeability could be determined between 0.05 and 0.076-cm thick flakes based on Tukey's HSD.

#### **4.1.1 Regression Analysis**

One of the stated objectives of this research was to develop an empirical equation that predicted permeability based on flake thickness and compaction ratio. The scatter plots

provided in Figures 4-1 to 4-3 clearly indicate that permeability and compaction ratio do not behave in a linear manner. To address the non-linear nature of the data the independent variables of compaction ratio and thickness were transformed using higher order terms of (compaction ratio)<sup>2</sup>, (compaction ratio)<sup>3</sup>, (thickness)<sup>2</sup> and (thickness)<sup>3</sup>. This polynomial model still failed to address the data appropriately so a further transformation was applied to the independent variable permeability using a natural logarithm. This data transformation was selected to prevent negative values for the permeability prediction. Once these treatments had been applied, stepwise multiple regression was performed to determine what parameters and their corresponding coefficients should be included in the model.

Table 4-4 provides the resulting model stepwise regression arrived at and its corresponding best of fit statistics R<sup>2</sup> and C(p). The coefficient of determination (R<sup>2</sup>) generally reflects a perfect fit to the data the closer it is to 1, it is the proportion of variability explained by the regressors in the model. C(p) is a measure of over-fit and under-fit balance (the smaller the better). The output from the statistical analysis software for the stepwise regression is provided in the appendix.

**Table 4-4. Stepwise regression results for variables entered into the model.**

Step	Variable Entered	Partial R-Squared	Model R-Squared	C(p)	F Value	Pr > F
1	C <sup>3</sup>	0.8459	0.8459	250.195	2179.29	<.0001
2	t <sup>2</sup>	0.0053	0.9012	20.8165	221.42	<.0001
3	C	0.0039	0.9051	6.5252	16.19	<.0001
4	C <sup>2</sup>	0.001	0.906	4.4186	4.11	0.0432

C = compaction ratio

T = flake thickness (cm)

By following the statistical principal of parsimony (less is more) the following Equation 8 was arrived at which had an R-squared of 0.9051 and a C(p) of 6.5252

$$\ln p = -16.896 - 0.896C - 1.23C^3 + 204.457t^2 \quad (8)$$

C = compaction ratio

t = flake thickness (cm)

p = superficial permeability ( $\text{m}^3 / \text{m Pa sec}$ )

Figure 4-4 provides the transverse permeability results for mats comprised of all flake thicknesses as well as the predicted values calculated using Equation 8 at similar compaction ratios. As indicated earlier, the mats comprised of thicker flakes have a higher permeability, which the predictive equation indicates. The predictive equation also shows that, at compaction ratios of 1.3 and higher, little difference in permeability is evident.

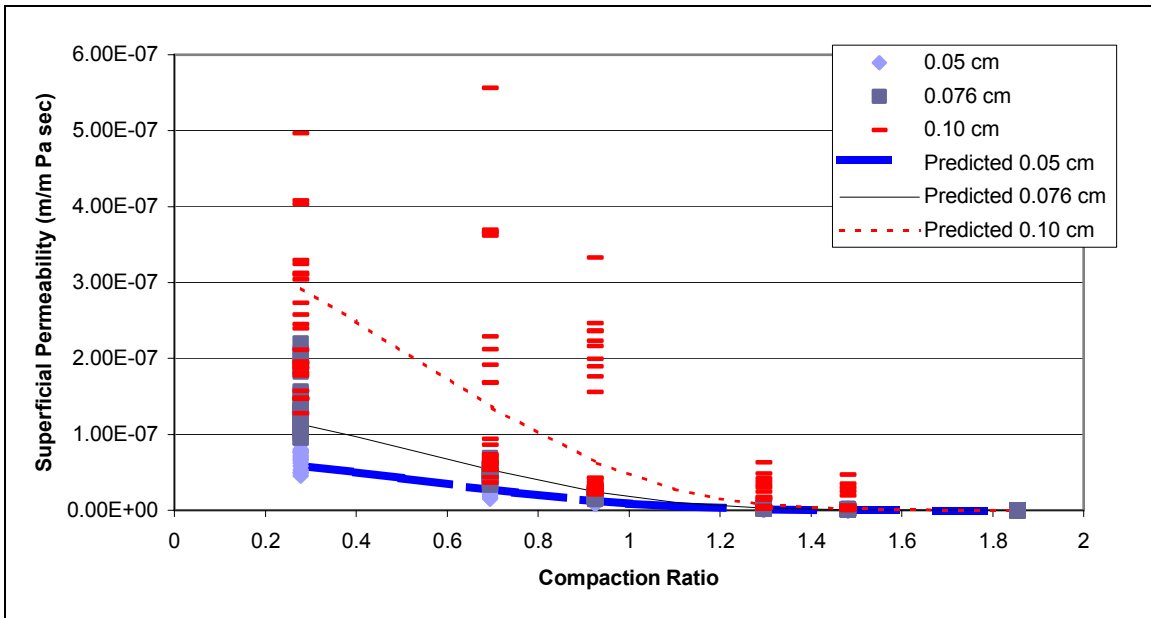


Figure 4-4. Scatter plot of actual transverse permeability measurements and predicted values for the same flake thickness based on Equation 6.

## 4.2 In-Plane Permeability

In-plane permeability measurements were conducted on five separate mats at various compactions ratios for three different flake thicknesses. Permeability measurements were conducted on separate mats for each compaction ratio. The in-plane permeability study includes results for permeability in the flake alignment direction, referred to as in-plane permeability parallel, and across the flake alignment direction, in-plane permeability perpendicular. For each mat, five sub-samplings were conducted based on different pressure differentials. In the case of permeability parallel and perpendicular, the mats comprised of 0.076-cm thick flakes served as the treatment control for comparative purposes.

### 4.2.1 In-Plane Permeability Parallel

Permeability decreases as compaction ratio is increased. Analysis of variance reveals that there is a significant difference in mean permeability between compaction ratios for mats comprised of 0.076-cm thick flakes ( $p < 0.0017$ ). Further analysis conducted using Tukey's HSD reveals that measured permeability for all compaction ratios is significantly different. As the compaction ratio is increased, the number of pathways available for flow is reduced. These pathways maybe reduced in size or some eliminated altogether. Figure 4-5 provides a scatter-plot of in-plane permeability parallel versus compaction ratio.

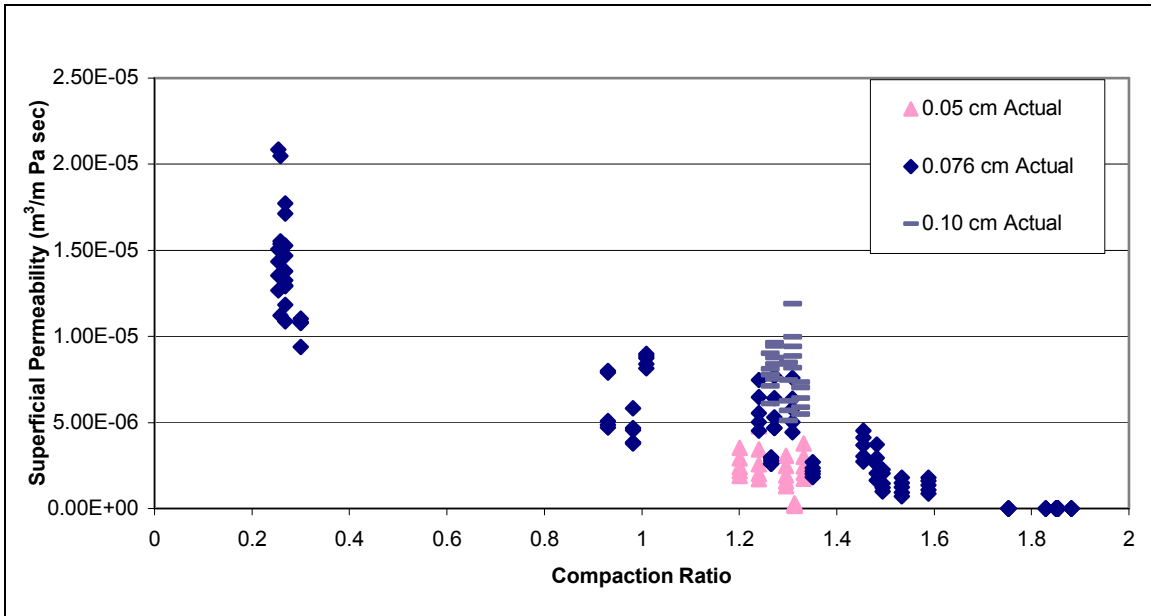


Figure 4-5. In-plane permeability parallel results for all flake thicknesses investigated.

**Table 4-5. Descriptive statistics for in-plane permeability parallel mats (m<sup>3</sup>/m Pa sec).**

Flake Thickness (cm)	0.076					0.05	0.10
Target Compaction Ratio	0.28	0.93	1.3	1.48	1.85	1.3	1.3
Mean	1.38E-05	6.42E-06	4.48E-06	2.07E-06	2.08E-09	2.08E-06	7.81E-06
Standard Deviation	2.94E-06	2.02E-06	1.88E-06	1.08E-06	3.76E-09	1.22E-06	1.63E-06
Minimum	9.38E-06	3.77E-06	1.81E-06	7.12E-07	2.49E-11	1.55E-07	5.12E-06
Maximum	2.09E-05	8.98E-06	7.69E-06	4.52E-06	1.4E-08	4.78E-06	1.19E-05
cov%	21.24	31.49	42.06	51.99	180.52	58.75	20.88

Table 4-5 provides the descriptive statistics for all in-plane permeability parallel mats tested. The coefficient of variation for the mats comprised of 0.076-cm thick flakes indicates that as compaction ratio increases, the variability in permeability increases. Analysis of variance reveals that permeability across flake thickness is significantly different ( $p < 0.022$ ). Further analysis using Tukey’s HSD indicates permeability is significantly different for all flake thicknesses.

Mats comprised of thicker flakes have higher permeability. This results from fewer flakes being required to form the mat, leading to a structure more conducive to flow. As the number of flakes is increased, the available pathways for flow become more tortuous, thus lowering the permeability. By increasing the number of flakes required to form a mat, the flow must negotiate more obstacles leading to mats with lower permeability based on a reduced flow rate. In contrast, as the compaction ratio increases, the available pathways for flow are reduced.

#### **4.2.2 In-Plan Permeability Perpendicular**

Analysis of variance reveals that there is a significant difference in mean permeability between compaction ratios for mats comprised of 0.076-cm thick flakes ( $p < 0.005$ ).

Further analysis conducted using Tukey’s HSD reveals that measured permeability for the target compaction ratios of 1.3 and 1.48 is not significantly different.

Analysis of variance reveals that permeability across flake thickness is significantly different ( $p < 0.011$ ). Further analysis using Tukey’s HSD indicates permeability is not significantly different for mats comprised of 0.05 and 0.076 cm thick flakes. Figure 4-6 provides a scatter-plot of in-plane permeability perpendicular versus compaction ratio.

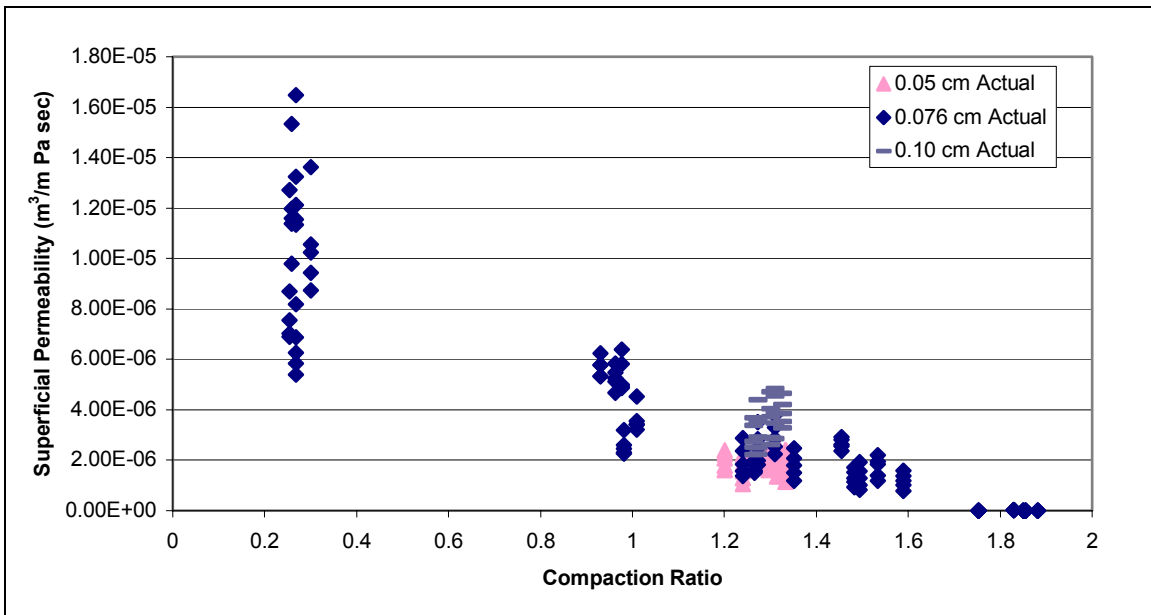


Figure 4-6. In-plane permeability perpendicular results for all flake thicknesses investigated.

Table 4-6. Discriptive statistics for in-plane permeability perpendicular mats ( $m^3/m Pa sec$ ).

Flake Thickness (cm)	0.076					0.05	0.1	
	Target Compaction Ratio	0.28	0.93	1.3	1.48	1.85	1.3	1.3
Mean		1.01E-05	4.51E-06	2.19E-06	1.64E-06	3.97E-09	1.87E-06	3.49E-06
Standard Deviation		2.97E-06	1.31E-06	6.92E-07	6.36E-07	7.83E-09	4.3E-07	8E-07
Minimum		5.39E-06	2.27E-06	1.19E-06	7.74E-07	4.96E-11	1.05E-06	2.23E-06
Maximum		1.65E-05	6.4E-06	3.78E-06	2.93E-06	2.4E-08	2.62E-06	4.85E-06
cov%		29.43	29.15	31.56	38.75	197.35	22.98	22.93

### 4.2.3 Regression Analysis

The in-plane permeability compaction ratio relationship presented in Figures 4-5 and 4-6 appears to be linear in nature. This linear relationship has led to difficulties in developing an empirical equation for predicted permeability based on compaction ratio and flake thickness as required by the objectives of this research. The problems arise when multiple regression is performed on the data, this results in a best of fit line that is linear. So the permeability predicted for high compaction ratios and thinner flakes is negative, which is not possible. An additional problem encountered with a linear equation is that the predicted permeability for flake thickness fails to converge as compaction ratio increases. A data transformation based on the natural log or higher order terms similar to that detailed in section 4.1.1 for transverse permeability fails to provide a satisfactory equation. To prevent the negative permeability prediction an interaction term based on flake thickness and compaction ratio was developed. The interaction term is  $[(t/C) * C^{1/3}]$ , ( $t$  = flake thickness,  $C$  = compaction ratio) this along with flake thickness was provided to SAS as the independent variables for multiple regression. Figures 4-7 and 4-8 present comparisons of predicted to actual permeability for in-plane permeability parallel and in-plane permeability perpendicular, respectively.

The resulting best-fit statistics for in-plane permeability parallel and perpendicular respectively, are presented in Table 4-7 and 4-8, followed by the resulting predictive equation.

**Table 4-7. In-plane permeability parallel summary statistics for stepwise regression.**

Step	Variable Entered	Partial R-Squared	Model R-Squared	C(p)	F Value	Pr > F
1	interaction	0.8778	0.8778	23.15	1177.67	<.0001
2	thickness	0.0152	0.893	2	23.15	<.0001

$$P = -0.0000235t + 0.00008857\left(\frac{t}{C} * \sqrt[3]{C}\right) \quad (9)$$

P = superficial gas permeability, m<sup>3</sup>/m Pa sec

t = flake thickness, cm

C = compaction ratio

**Table 4-8. In-plane permeability perpendicular summary statistics for stepwise regression.**

Step	Variable Entered	Partial R-Squared	Model R-Squared	C(p)	F Value	Pr > F
1	interaction	0.8549	0.8549	72.414	1025.12	<.0001
2	thickness	0.0428	0.8977	2	72.41	<.0001

$$P = -0.00002725t + 0.00006832\left(\frac{t}{C} * \sqrt[3]{C}\right) \quad (10)$$

P = superficial gas permeability, m<sup>3</sup>/m Pa sec

t = flake thickness, cm

C = compaction ratio

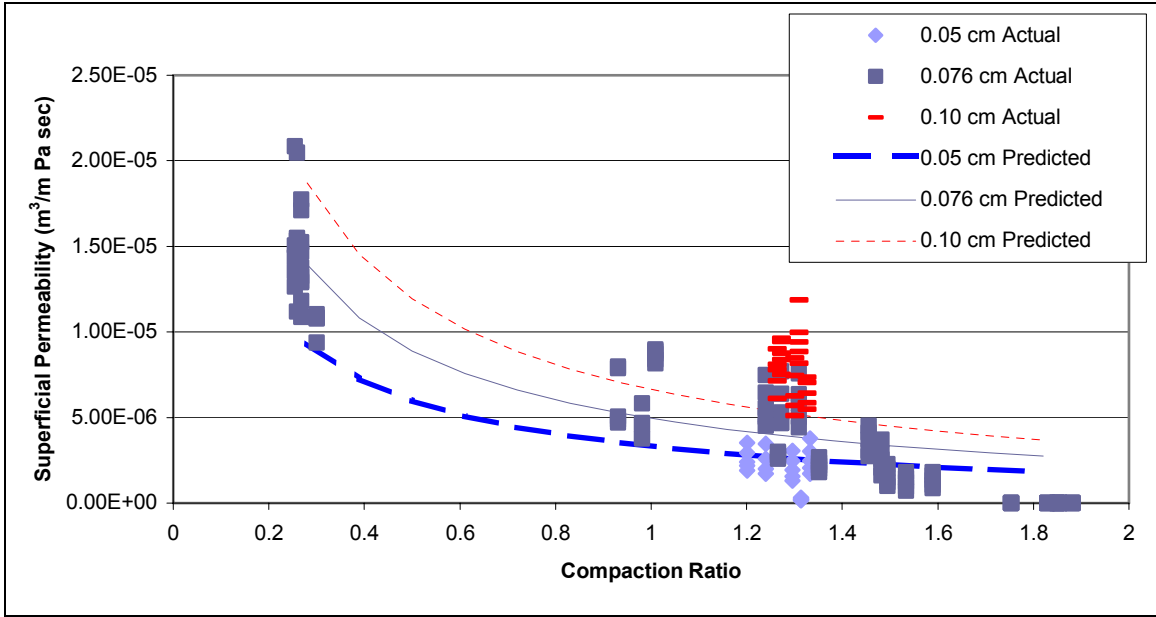


Figure 4-7. In-plane permeability parallel actual results and predicted values for all flake thicknesses tested based on Equation 9.

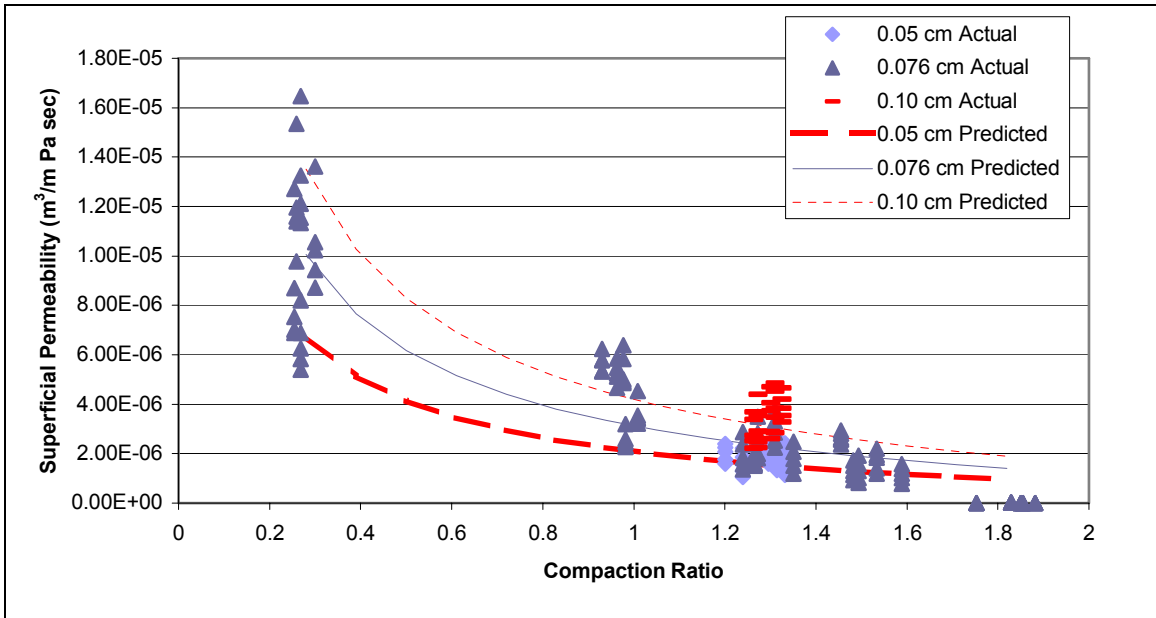


Figure 4-8. In-plane permeability perpendicular actual results and predicted values for the same flake thickness based on Equation 10.

In order for Equations 9 and 10 to be valid, it must be assumed that the flake thickness results from the fractional factorial experiment are consistent through the entire range of

compaction ratios. Mats comprised of thicker flakes result in higher permeability measurements, this relationship must hold true for the equations to be valid. The transverse permeability results lend credence to this assumption.

### ***4.3 Transverse and In-Plane Permeability Comparisons***

Analysis of variance reveals significant differences for comparisons of in-plane permeability parallel to perpendicular ( $p < 0.019$ ) for the three different flake thicknesses. Tukey's HSD reveals that no significant difference exists for in-plane permeability parallel for mats comprised of 0.05 and 0.076 cm thick flakes and in-plane permeability perpendicular mats comprised of 0.05 cm thick flakes.

The flow encountered in transverse permeability measurements was much more restricted. The flow first encounters a fairly wide octagonal opening where possibility several flakes meet (Figure 4-9). The length of uninterrupted flow might only be the thickness of a flake then the flow must transverse the flake face itself. This travel around the flake faces is what leads to the reduced permeability encountered in measurements through the thickness of the mat. In contrast flow in-plane permeability parallel encounters narrow slit like openings between the flakes. Once through these openings the flow has long distances without interruption between the flake layers, possibly as long as a flake itself. These long paths of uninterrupted flow leads to in-plane permeability being much higher than transverse. In the case of permeability across the flake alignment direction, the pathway of uninterrupted flow is still longer than through the thickness,

again resulting in higher permeability. However, in comparison to in-plane permeability parallel the pathway available for uninterrupted flow is much shorter, therefore leading to lower permeability.



**Figure 4-9. Between flake openings available for transverse flow.**

The pathways available for flow and the influence of increasing compaction ratio are illustrated in Figure 4-10. The reduction in pathways available for flow as compaction ratio increases is evident. Figure 4-11 illustrates how transverse flow and in-plane flow could possibly occur via one particular pathway.



Figure 4-10. The progression from low to high compaction ratios. A. 0.28, B. 0.93, C. 1.48.

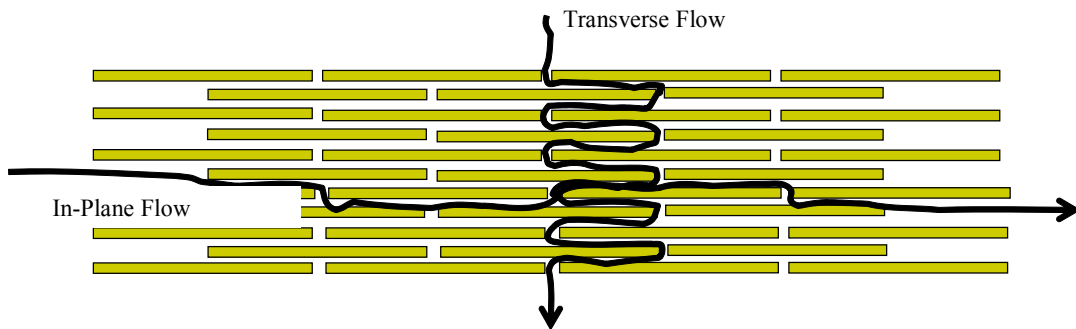


Figure 4-11. An approximation of the available transverse and in-plane flowpaths.

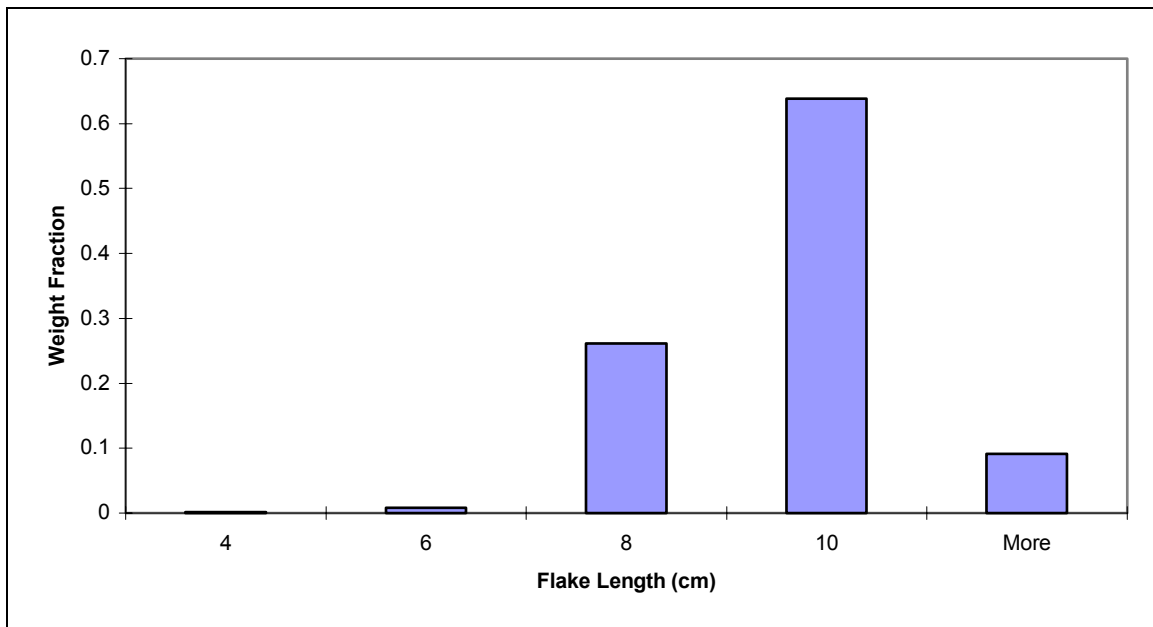
#### 4.4 Commercial Flake Comparison

The flakes used to make the mats for the commercial versus experimental comparisons were classified into five size categories. This was done in an effort to address any flake size influence on permeability that could manifest itself in the results.

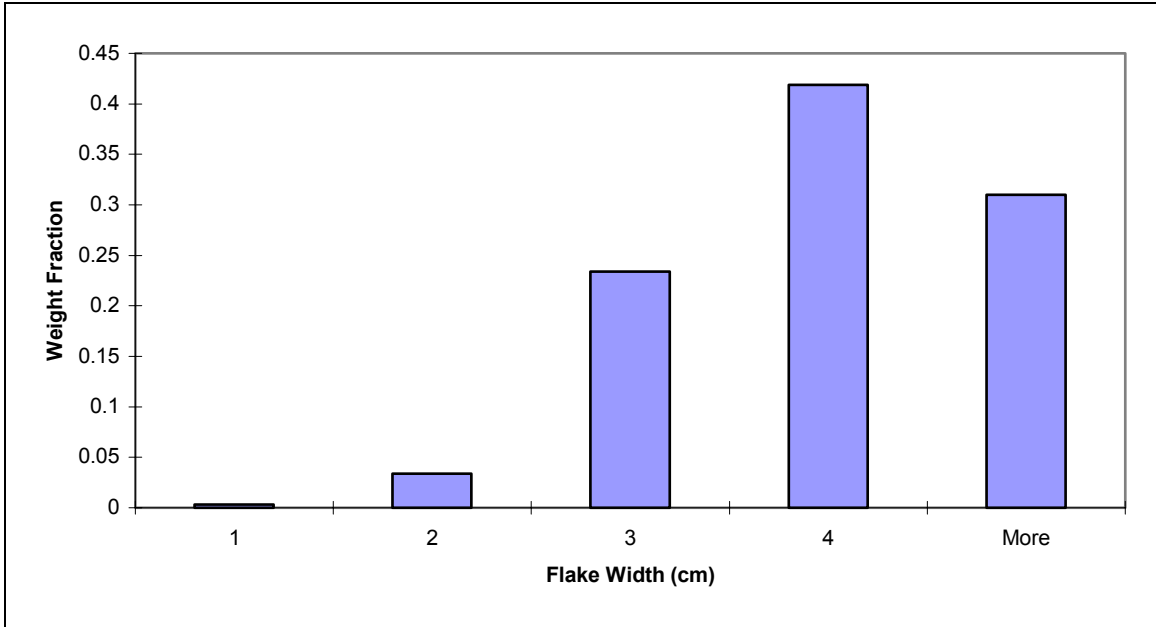
**Table 4-9. Commercial flake descriptive statistics.**

n = 500	Length (cm)	Width (cm)	Thickness (cm)	Density (Kg/m <sup>3</sup> )
Mean	8.40	1.57	0.08	494
Standard Deviation	2.76	1.12	0.03	137
C.O.V. (%)	32.83	71.35	39.71	28

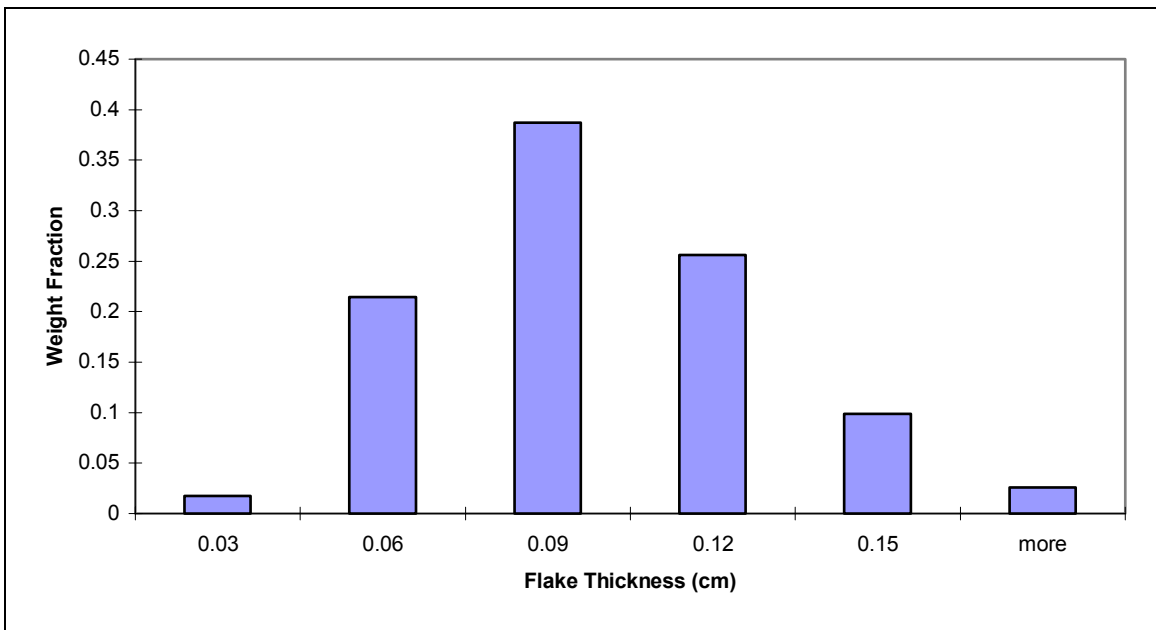
Table 4-9 provides the resulting average flake size and density. The average flake density was then used to determine compaction ratio. Figures 4-12 through 4-15 provides a frequency distribution for the commercial flake length, width, thickness, and density respectively, based on the weight fraction in each range.



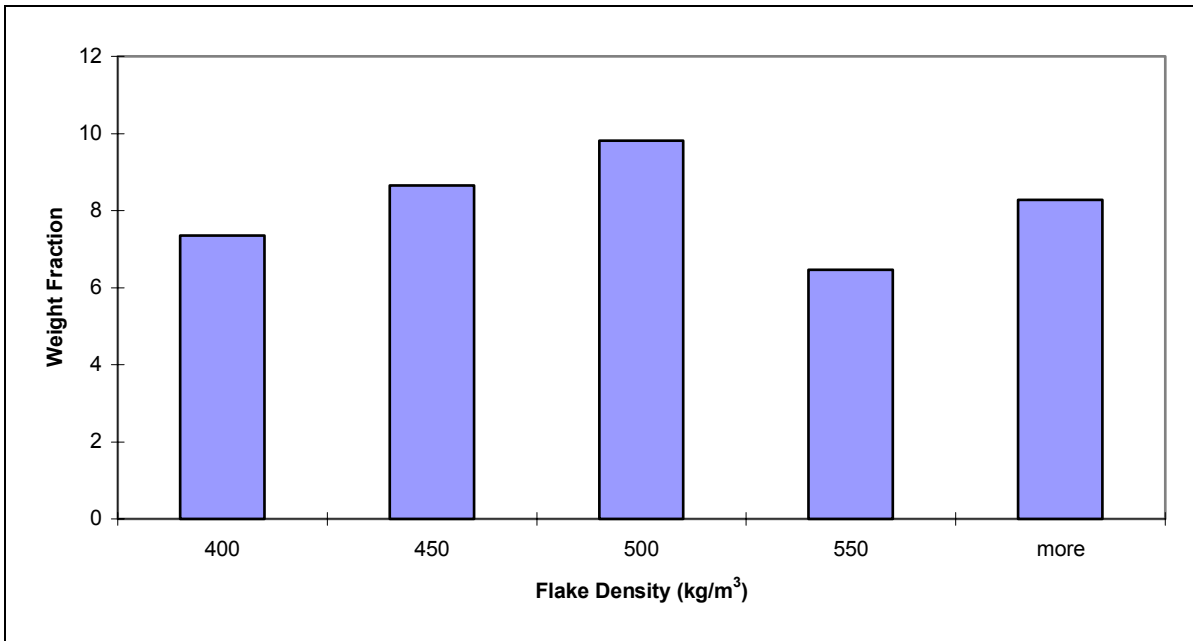
**Figure 4-12. Frequency distribution of flake length for commercial flakes.**



**Figure 4-13. Frequency distribution of flake width for commercial flakes.**

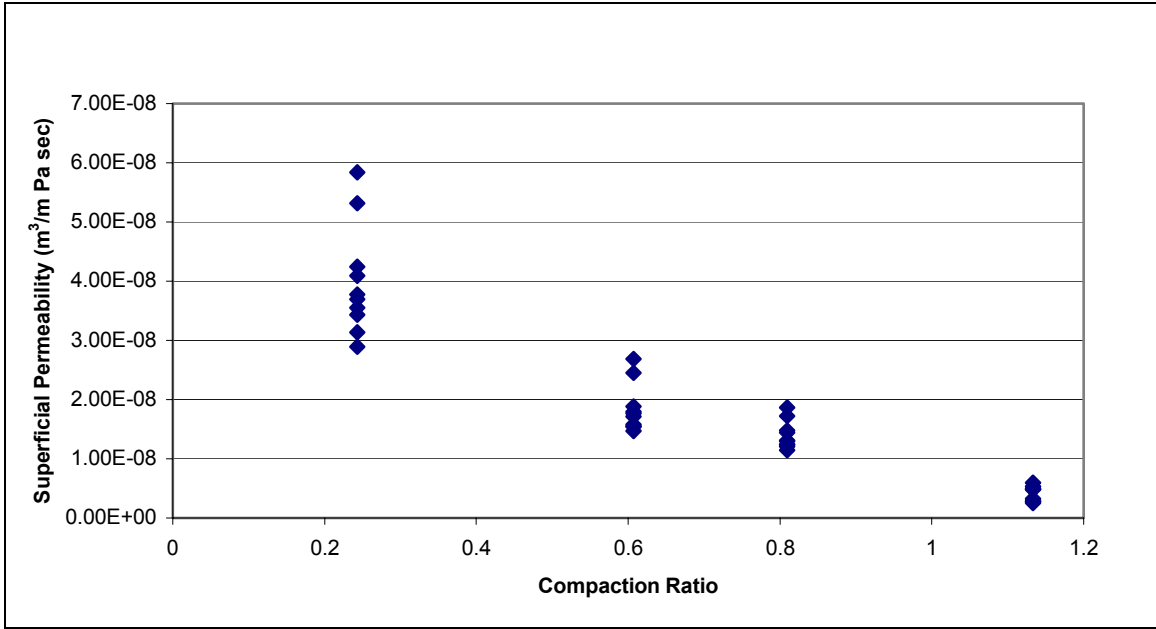


**Figure 4-14. Frequency distribution for flake thickness of commercial flakes.**



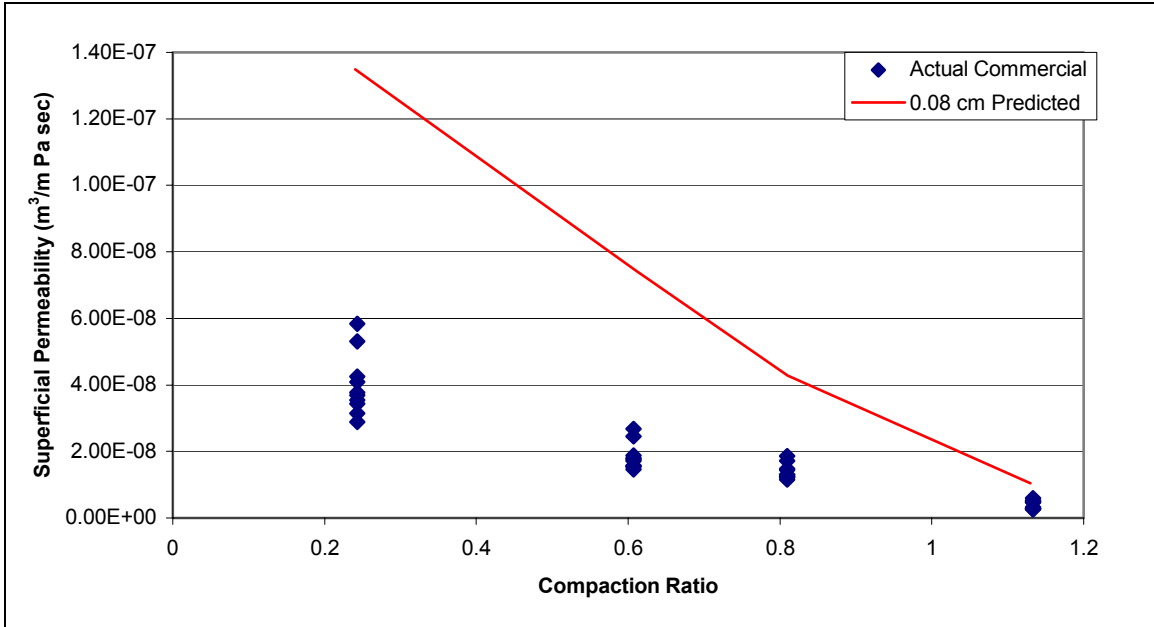
**Figure 4-15. Frequency distribution for flake density of commercial flakes.**

Figure 4-16 provides a scatter plot of observed permeability versus compaction ratio for commercial flake mats. The trend observed in the commercial flake mats is similar to that in the experimental flake mats. Based on the results from the experimental mats, observations beyond a compaction ratio of 1.2 were deemed unnecessary because no statistically significant difference in permeability could be observed.



**Figure 4-16. Commercial flake transverse permeability.**

Figure 4-17 compares actual permeability measured to the predicted permeability based on Equation 8. Based on the average commercial flake thickness, the predicted permeability is higher than what was observed.



**Figure 4-17. Commercial flake transverse permeability results and the permeability predicted by Equation 6 for the average thickness.**

The discrepancy in observed and predicted permeability can be explained by the number of large flakes used in the manufacture of the commercial mats. Figure 4-13 details the occurrence of these larger flakes in the form of a weight fraction histogram of various size ranges. Only 23 percent of the commercial flake mats were comprised of flakes similar in width to the experimental flake mats, 70 percent of the flakes were larger.

The presence of large flakes in the commercial mats would lead to areas of reduced permeability. The flow that must traverse these areas encounters longer, and more tortuous flow paths, leading to an overall reduction in permeability. In the localized areas of these larger flakes, the flow spends more time traveling in the plane of the mat than through its thickness. This reduces the flow rate, leading to a decrease in permeability.

In comparison, the flow occurring in mats comprised of smaller flakes does not spend time on extended detours around the flakes.

Figure 4-18 shows the in-plane permeability parallel measured for mats comprised of commercial flakes. These mats exhibit a similar trend to those mats comprised of the experimental flakes.

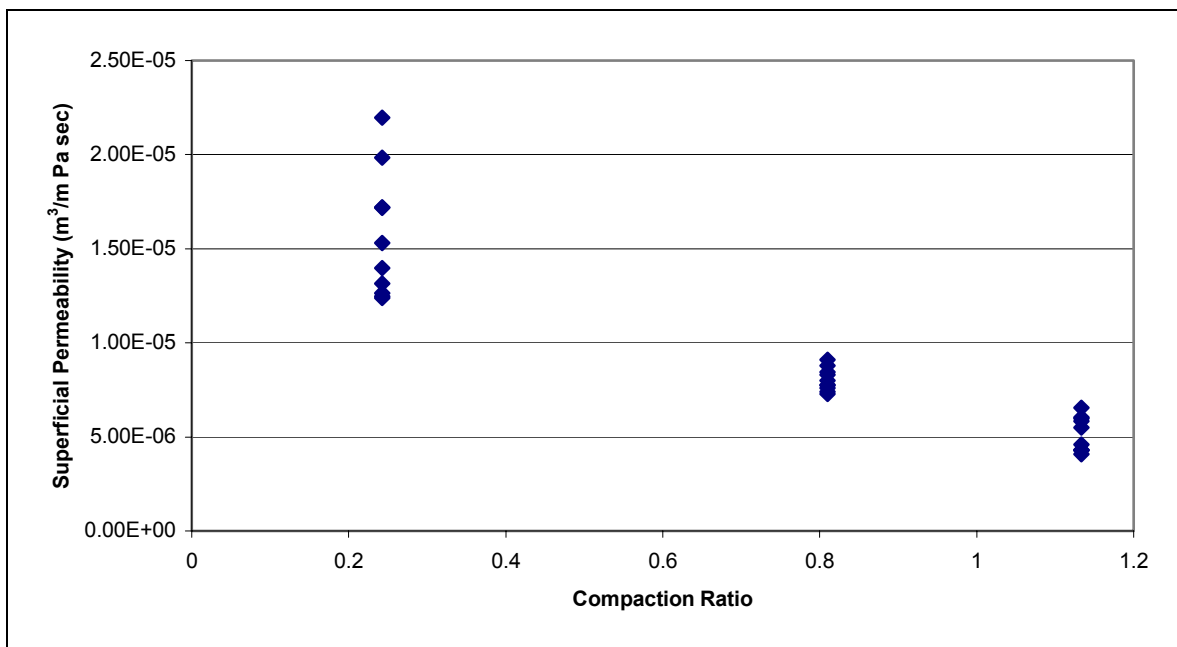


Figure 4-18. Commercial flake in-plane permeability parallel.

Figure 4-19 provides the actual in-plane permeability as well as the predicted in-plane permeability parallel.

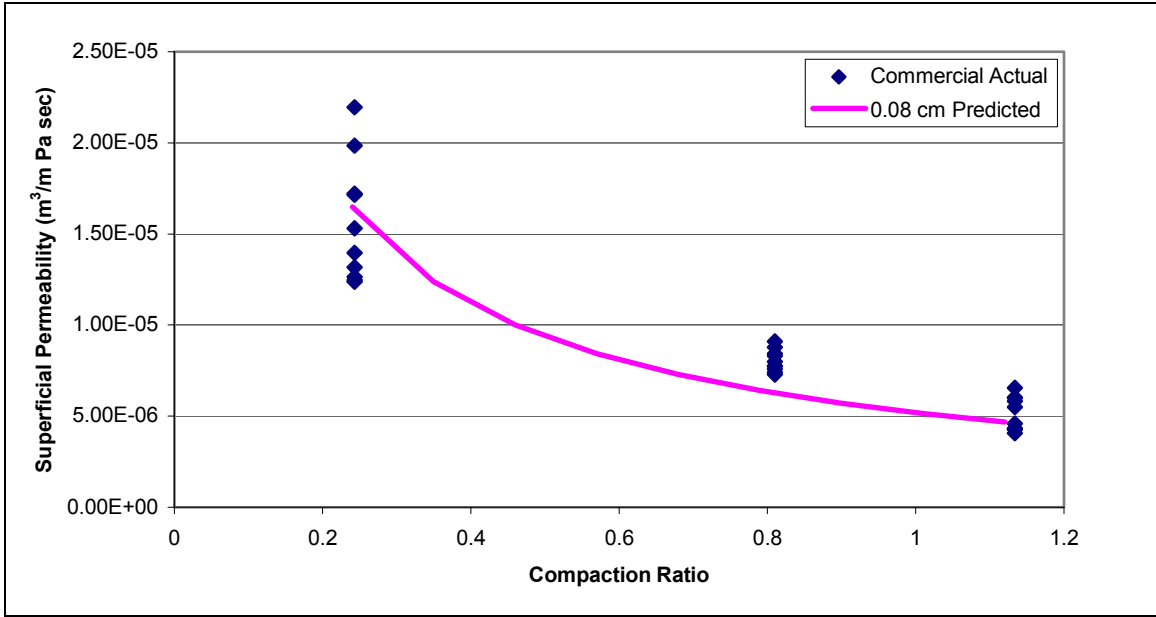


Figure 4-19. Results for in-plane permeability parallel for commercial flakes and predicted permeability based on Equation 9 for average thickness.

Figure 4-20 shows the in-plane permeability perpendicular measured for mats comprised of commercial flakes. These mats exhibit a similar trend to those mats comprised of the experimental flakes.

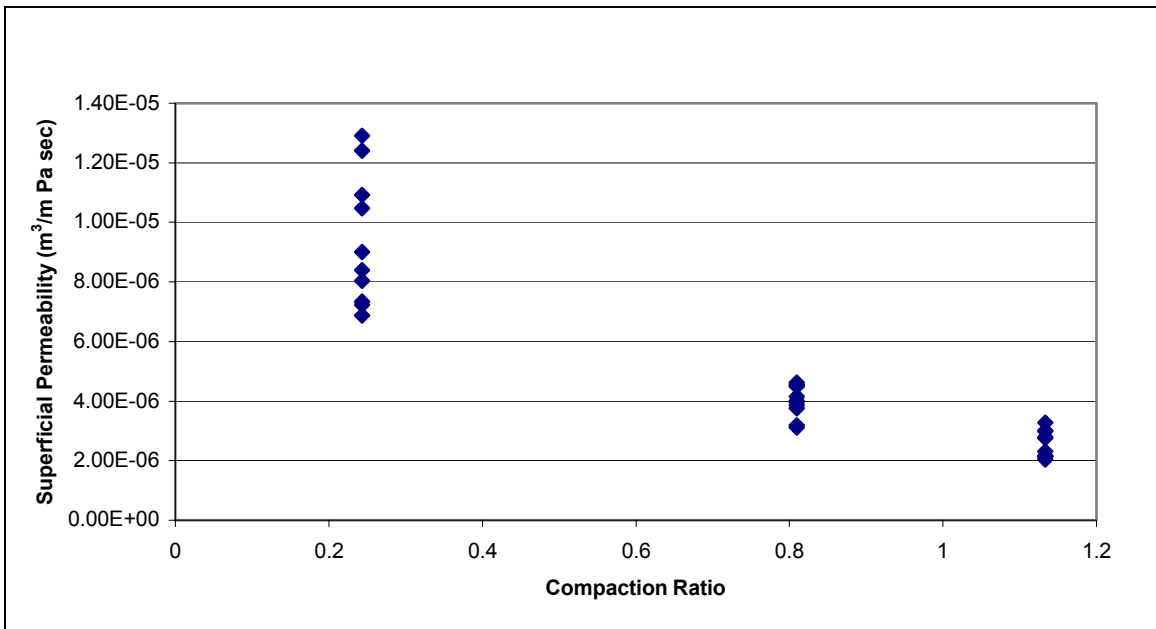
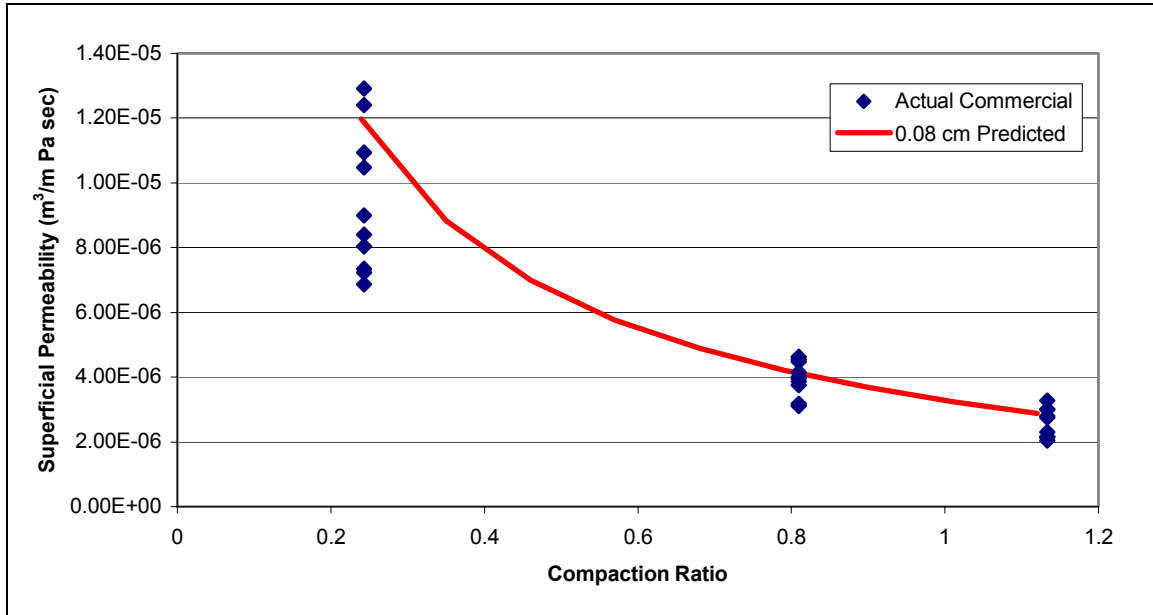


Figure 4-20. Commercial flake in-plane permeability perpendicular.

Figure 4-21 provides the actual in-plane permeability as well as the predicted in-plane permeability perpendicular.



**Figure 4-21. Commercial flake in-plane permeability perpendicular and predicted permeability based on Equation 10 at the average flake thickness.**

It is clear from the results in this section that transverse permeability is strongly influenced by flake width given the reduced permeability encountered compared to that predicted. However, it is also clear from this section that in-plane permeability parallel and perpendicular is not as dependent on flake width, since the predicted permeability adequately describes the actual based on average flake thickness. No means was available to restrict the density ranges in the commercial flake mats; the compaction ratio used was based on an average density. This could possibly lead to areas within the mat that had higher compaction ratios than the average, therefore lowering the permeability in the transverse direction and contributing to the lower permeability than predicted.

## **4.5 Previous Research Comparison**

Von Haas et al. (1998) conducted previous work on the density-based influence on the permeability of OSB. From this research, Equation 5 was developed to predict permeability based on various mat densities and resin contents of OSB panels. Scotts pine (*Pinus sylvestris*) flakes were obtained from a commercial facility and used in the manufacture of these panels. The species density was never determined, so the influence of compaction ratio on permeability was not possible. Given this limitation, comparing the prediction ability of Equation 8 to that developed by Von Haas is difficult. In an effort to address the compaction ratio limitation, a range of commonly encountered densities for the species used in the study was determined to be 470-530 kg/m<sup>3</sup> (Wimmer 1995). The corresponding compaction ratios were calculated. In Figure 4-22, the low compaction data presented was based on the ratio of panel density used in the study to the high-density range encountered in the species. The high compaction ratios were based on the low-density end of the range encountered in the species.

It is clear from the figure that a wide range in compaction ratios is possible, but for each pair encountered, the permeability predicted is the same. As compaction ratio increases, the number of voids and interconnecting pathways available for flow decreases, leading to lower permeability, this reduction in permeability is not seen in the predictive power of Equation 5. Using Equation 8 to predict permeability, based on the same compaction ratios, provides similar results for mats comprised of 0.10-cm thick flakes above the compaction ratio of 0.8. Equation 5 was developed based on finished mats containing

adhesive and results could only be determined from mat densities of  $400 \text{ kg/m}^3$  or higher. Given these restrictions, comparisons below the compaction ratio of 0.8 are impossible.

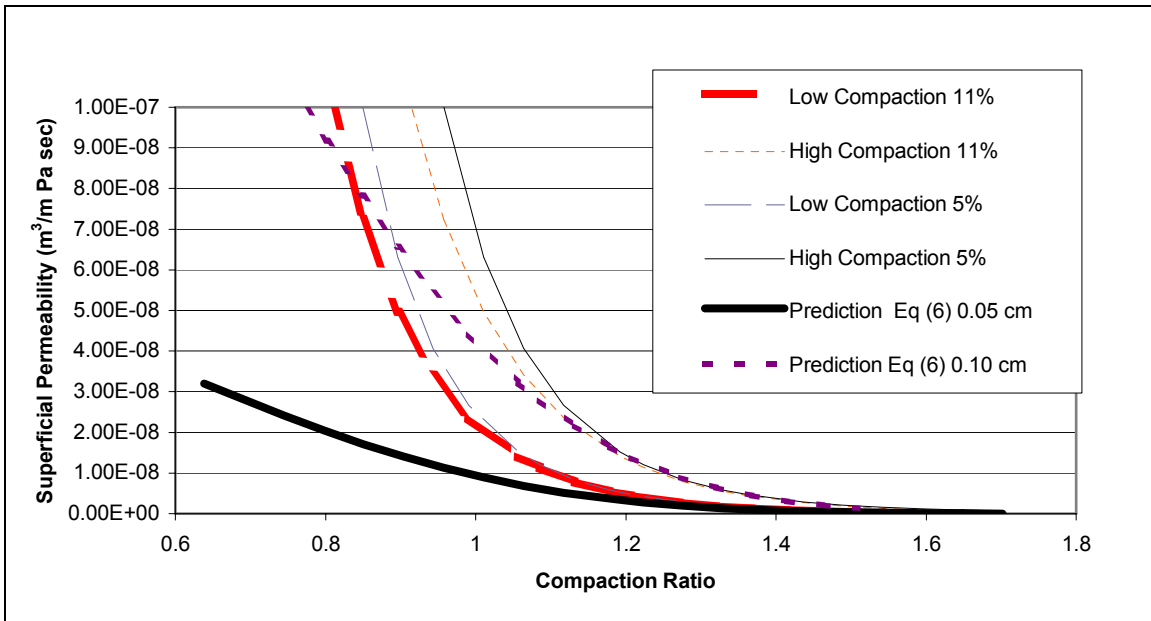


**Figure 4-22.** Transverse permeability predictions based on Von Haas' equation corresponding to the range of densities commonly encountered in *Pinus sylvestris* as well as the influence of resin content (5 and 11%). Results from Equation 8 are also presented based on the same compaction ratios at a flake thickness of 0.05-cm and 0.10-cm.

The importance of compaction ratio is evident in Figure 4-22. If a target mat density of  $600 \text{ kg/m}^3$  is desired and a low-density species is used as a raw material, the target compaction ratio could be quite high and the resulting permeability extremely low. If the same mat is made using a higher density species, the target compaction ratio could be much lower, resulting in a finished mat with a higher permeability.

Figure 4-23 provides the predicted in-plane permeability parallel based on Equation 5 compared to that predicted by Equation 9. For the prediction based on Equation 5 high and low compaction ratios are presented based on the high and low end of the species

density range. Figure 4-24 provides the same information for in-plane permeability perpendicular but the comparison is made between the permeability prediction of Equation 5 and that of Equation 10.

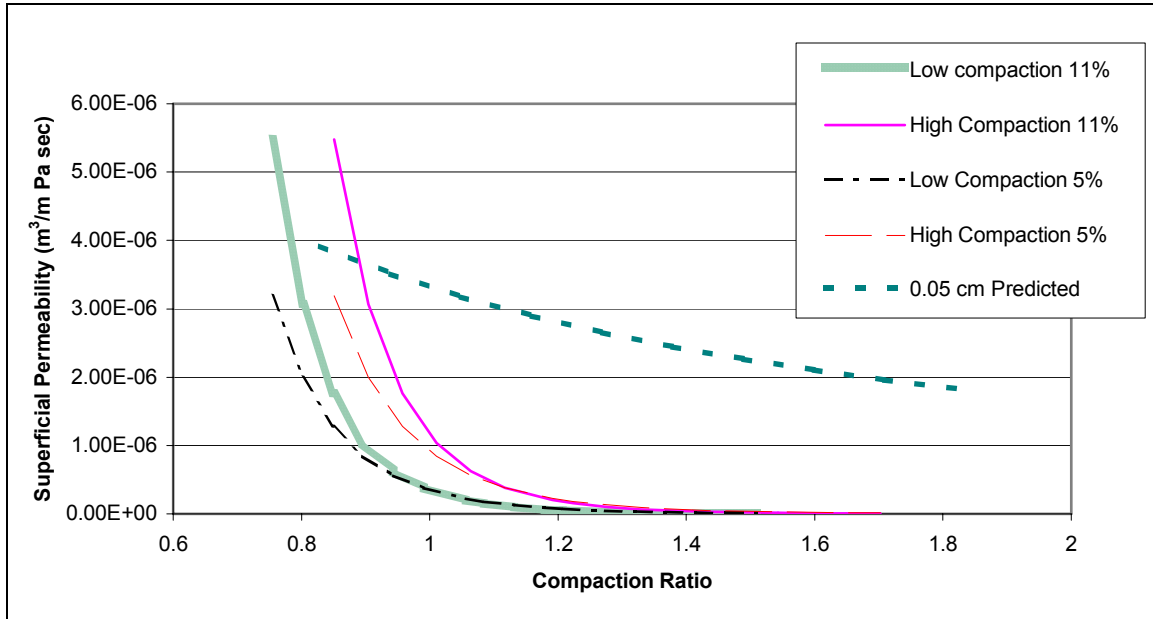
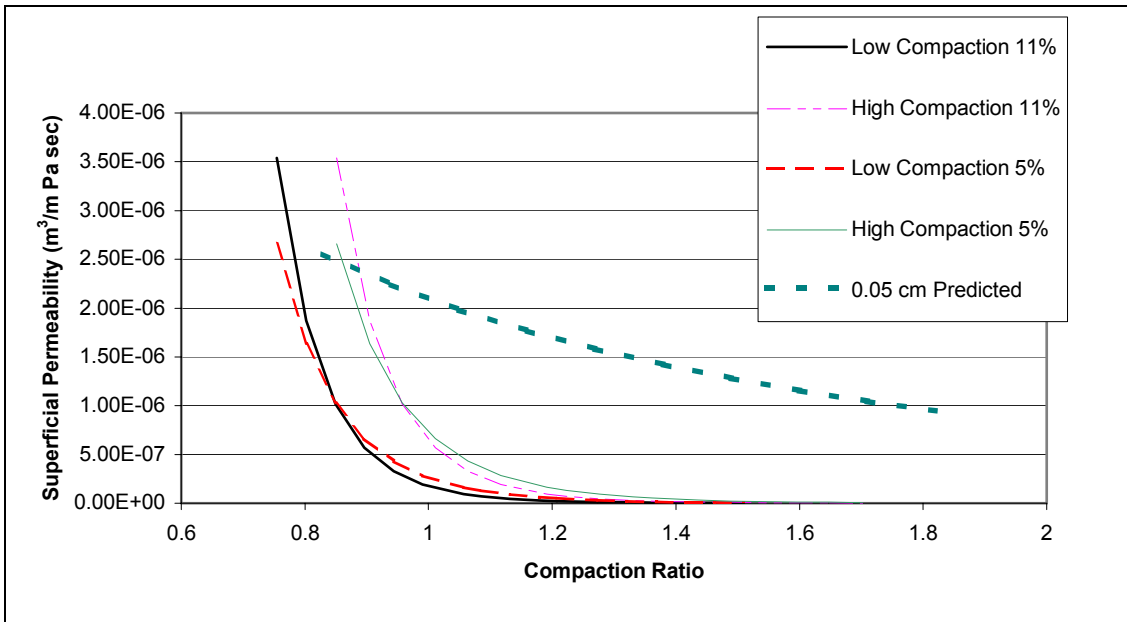


Figure 4-23. In-plane permeability parallel predictions based on Von Haas' equation at the high and low range end of densities commonly encountered in *Pinus sylvestris* compared to permeability predictions based on Equation 9.



**Figure 4-24. In-plane permeability perpendicular predictions based on Von Haas' equation at the high and low range end of densities commonly encountered in *Pinus sylvestris* compared to permeability predictions based on Equation 10.**

As can be seen in Figures 4-23 and 4-24 the in-plane permeability predictions based on Equations 9 and 10 do not predict a similar permeability to that of Equation 5. Equation 5 being used to predict the transverse and in-plane permeability most likely causes this comparison problem, because it is doubtful that transverse and in-plane permeability exhibit the same trend. The only adjustments to the equation are based on coefficients for the principal directions. The same equation was developed to predict permeability in the principal directions for fiberboard and particleboard. Again it is doubtful that three different wood-particle composites would exhibit the same trend for transverse and in-plane permeability.

## **5 Summary, Conclusions and Recommendations**

### **5.1 Summary**

The first objective of this project was to design and build an apparatus for measuring transverse (through the thickness) and in-plane permeability of oriented strandboard mats during the pressing operation. Two different designs were used to meet this objective, one for transverse permeability and one for in-plane permeability.

The second objective was to determine how permeability is influenced by changes in mat density during pressing. Transverse permeability decreases rapidly as the compaction ratio is increased, but at a compaction ratio of 1.3 and above, no statistically significant difference in permeability can be detected. In-plane permeability parallel and perpendicular exhibited decreasing permeability with increasing compaction ratio, with the statistical differences being significant throughout the entire range of compaction ratios tested. At low compaction ratios, the voids present in the mat exhibit a high degree of connectivity, thus contributing to the higher permeability. As the compaction ratio is increased, the pathways available for flow are reduced, thus lowering the permeability.

The third objective was to determine how permeability is influenced by flake thickness and alignment. Transverse and in-plane permeability were higher for mats comprised of thicker flakes. This is caused by a reduction in flow-path tortuosity (the flow must traverse fewer obstacles). In-plane permeability was higher in the flake alignment

direction. This is due to the available flow-paths, which are longer before the flow encounters obstructions that must be negotiated.

The final objective of this project was to develop an empirical equation that predicts permeability based on flake thickness and compaction ratio. Three different equations were developed that predicted permeability, one for each of the principal directions.

## **5.2 Conclusions**

The following conclusions may be drawn from this research:

- Compaction ratio is the most important factor influencing oriented strandboard mat permeability.
- As compaction ratio increases permeability decreases.
- Mats comprised of thicker flakes have higher permeability.
- Permeability is higher in the flake alignment direction.

From this research, manufacturers can gain a better understanding of when to inject steam during the steam-injection pressing operation. This research could also lead to the manipulation of vertical density gradients in order to better control the in-plane permeability for conventional hot-pressing. The regression equations have been implemented in the hot-pressing simulation model (WBCSim). They could also be used by others in future hot-press models.

### **5.3 Recommendations**

Further study in the field of oriented strandboard permeability should address what influence moisture content has. The influence of flake width or size on mat permeability should be determined in future research. The influence of adhesives and additives such as wax should be considered in future research.

### **5.4 Limitations**

The results of this project are limited by the following. It is assumed that all of the samples measured lacked a pronounced vertical density gradient. The samples for the highest compaction ratio measurements contained adhesive, it is assumed that this had a negligible influence on the measured permeability. This was actually the case in the transverse permeability results, because no statistically significant difference could be determined at a compaction ratio of 1.3 and above. The in-plane permeability predictive equations were determined based on an experiment design that considered additional flake thicknesses only at a compaction ratio of 1.30. The regression analysis assumed the influence of flake thickness was the same within the range of compaction ratios studied.

## 6 References

- Beiser, A. 1973. Physics. Cummings Publishing Co. Menlo Park CA.
- Bolton, A.J., P.E. Humphrey. 1988 The hot pressing of dry-formed wood-based composites. Part I. A review of the literature, identifying the primary physical process and the nature of their interaction. *Holzforchung* 42(6):403-406.
- Bolton, A.J., P.E. Humphrey. 1994. The permeability of wood-based composite materials. Part I. A review of the literature and some unpublished work. *Holzforchung* 48:95-100.
- Bolton, A.J., P.E. Humphrey, P.K. Kavvouras. 1989a. The hot pressing of dry formed wood-based composites. Part III. Predicted vapour pressure and temperature variation with time, compared with experimental data for laboratory boards. *Holzforchung* 43(4): 265-274.
- Bramhall, G. 1971. The validity of Darcy's Law in the axial penetration of wood. *Wood Science and Technology*. 5(1971)121-134.
- D'Onofrio, M. 1994. The superficial gas permeability of northeastern conifers and aspen flake composites. MS. Thesis. University of Maine.
- Garcia, P. 2002. Three-dimensional heat and mass transfer during oriented strandboard hot-pressing. PhD. Dissertation. University of British Columbia, Vancouver, BC. 254 p.
- Garcia, P.J., S. Avramidis, F. Lam. 2001 Internal temperature and pressure responses to flake alignment during hot-pressing. *Holz als Roh und Werkstoff* 59:272-275.
- D. J. Gardner. 2002. Flow through fabrics. Presentation, University of Maine.
- Geimer, R.L., H.M. Montrey, W. F. Lehmann. 1975. Effects of layer characteristics on the properties of three layer particleboards. *Forest Products Journal* 25(3):19-29.
- Haas., G., A. Steffen, A. Fruhwald. 1998. Untersuchungen zur Permeabilitat von Faser-, Span- und OSB-Matten fur Gase. *Holz als Roh und Werkstoff* 56:386-392.
- Haas., G., 1998. Investigations of the hot pressing of wood composite mats under special consideration of the compression behavior, the permeability, the temperature-conductivity and the sorption speed. (In German). Ph.D thesis, University of Hamburg, Germany.
- Haselein, C. R. 1998. Numerical simulation of pressing wood-fiber composites. PhD. Thesis. Oregon State University, Corvallis, OR.

Humphrey, P.E. 1982. Physical aspects of wood particleboard manufacture. Ph.D. Thesis. University of Wales, U.K.

Humphrey, P.E. and A.J. Bolton. 1989. The hot pressing of dry-formed wood-based composites. Part II. A simulation model for heat and moisture transfer and typical results. *Holzforchung* 43(3):199-206.

Joslyn, D.W. 1972. Treatability and Longitudinal Air Permeability of Commercial Species Grown in Chile. MS. Thesis. V.P.I. & S.U. Blacksburg, VA.

Kamke, F.K. and L.J. Casey. 1988a. Gas pressure and temperature in the mat during flakeboard manufacture. *Forest Products Journal*. 38(3):41-43.

Kamke, F.K. and L.J. Casey. 1988b. Fundamentals of flakeboard manufacture: internal-mat conditions. *Forest Products Journal*. 38(6):38-44.

Kamke, F.K. and M.P. Wolcott. 1991. Fundamentals of flakeboard manufacture: wood-moisture relationship *Wood Science and Technology* 25:57-71.

Kamke, F.K. and S.C. Zylkowski. 1989. Effects of wood-based panel characteristics on thermal conductivity. *Forest Products Journal*. 39(5):19-24.

Kays, M.W. and M. E. Crawford. 1993. *Convective Heat and Mass Transfer*. McGraw-Hill. New York, NY.

Kelly, M.W. 1977. Critical literature review of relationships between processing parameters and physical properties of particleboard. USDA. Forest Service, Forest Products Laboratory, General Technical Report FPL-10

Lenth, C. A. 1994. Investigations of Flakeboard Mat Consolidation. MS. Thesis. VPI & SU., Blacksburg, VA

Neiva, A., L. Goldstein Jr. 2003. A procedure for calculating pressure drop during the build-up of dust filter cakes. *Chemical Engineering and Processing*. 42(2003) 495-501.

Palardy, R.D., B.A. Haataja, S.M. Shaler, A.D. Williams, and T.L. Laufenberg. 1989. Pressing of wood composite panels at moderate temperature and high moisture content. *Forest Products Journal* 39(4):27-32.

Petty, J.A. and R.D. Preston. 1969. The dimensions and number of pit membranes in conifer wood. *Proc. R. Soc. Lond. B* 172:137-151.

Pichelin, F., A. Pizzi, A. Fruhwald, P. Triboulot. 2001. Exterior OSB preparation technology at high moisture content Part 1: Transfer mechanisms and pressing parameters. *Holz als Roh und Werkstoff* 59:256-265.

- Siau, J.F. 1971. Flow in Wood. Syracuse University Press. Syracuse, NY.
- Siau, J.F, 1984. Transport Processes in Wood. Springer-Verlag, New York, NY.
- Siau, J.F. 1995. Wood: Influence of Moisture on Physical Properties. Department of Wood Science and Forest Products, VPI & SU Blacksburg, VA.
- Siau, J.F., J.A. Petty. 1979. Corrections for capillaries used in permeability measurements of wood. Wood Science and Technology. 13:179-185.
- Skaar, C. 1988. Wood-Water Relations. Springer-Verlag. Berlin.
- Smith, D. C. 1982. Wafer board press closing strategies. Forest Products Journal 32(3):40-45.
- Strickler, M.D. 1959. Effects of press cycle and moisture content on properties of Douglas-fir flakeboard. Forest Products Journal. 9(7):203-215.
- Suchsland, O. 1967. Behavior of a particleboard mat during the press cycle. Forest Products Journal. 17(2)51-57.
- Suleiman, B.M., J. Larfeldt, B. Leckner, M. Gustavsson. 1999. Thermal conductivity and diffusivity of wood. Wood Science and Technology. 33:465-473.
- Thomen, H. 2001. Modeling the Physical Process in Natural Fiber Composites During Batch and Continuous Pressing. PhD. Thesis. Oregon State University, Corvallis OR.
- Torrey, K.S. 2001. Influence of Thermally Conductive Fillers on Physical Properties of Waferboard. MS, Thesis, Michigan Technological University.
- Ward, R.J. and C. Skaar. 1963. Specific heat and conductivity of particleboards as functions of temperature. Forest Products Journal. 13(1):31-38.
- Wimmer, R., 1995. Intra-annual cellular characteristics and their implications for modeling softwood density. Wood and Fiber Science. 27(4):413-420.
- Wood Handbook: Wood as an Engineering Material. 2002. U.S.D.A. Agriculture Handbook:72. Washington D.C.
- Zavala, D., P.E. Humphrey. 1996. Hot-pressing veneer-based products: The interaction of physical processes. Forest Products Journal. 46(1):69-79.

## Appendix

**Table A- 1. Analysis of variance for transverse permeability on mats comprised of 0.05-cm thick flakes.**

Source	Sum of Squares	Degree of Freedom	Mean Square	P-value
Treatments	1.01E-13	4	2.50E-14	0.005
Experimental Error	4.40E-15	4	1.11E-15	
Observation Error	7.57E-15	116	6.53E-17	
Total	1.13E-13	124		

**Table A- 2. Analysis of variance for transverse permeability on mats comprised of 0.076-cm thick flakes.**

Source	Sum of Squares	Degree of Freedom	Mean Square	P-value
Treatments	3.65E-13	5	7.30E-14	0.001
Experimental Error	5.85E-15	4	1.46E-15	
Observation Error	2.44E-14	140	1.74E-16	
Total	3.95E-13	149		

**Table A- 3. Analysis of variance for transverse permeability on mats comprised of 0.10-cm thick flakes.**

Source	Sum of Squares	Degree of Freedom	Mean Square	P-value
Treatments	1.00E-12	4	2.51E-13	0.25
Experimental Error	4.87E-13	4	1.22E-13	
Observation Error	4.61E-13	116	3.97E-15	
Total	1.95E-12	124		

**Table A- 4. Analysis of variance for in-plane permeability parallel.**

Source	Sum of Squares	Degree of Freedom	Mean Square	P-value
Treatments	2.84E-09	4	7.09E-10	0.0017
Experimental Error	7.02E-11	4	1.75E-11	
Observation Error	3.07E-10	106	2.90E-12	
Total	3.22E-09	114		

**Table A- 5. Analysis of variance for in-plane permeability parallel across all flake thicknesses.**

Source	Sum of Squares	Degree of Freedom	Mean Square	P-value
Treatments	4.15E-10	2	2.07E-10	0.022
Experimental Error	7.15E-11	4	1.80E-11	
Observation Error	1.13E-10	68	1.70E+12	
Total	6.00E-10	74		

**Table A- 6. Analysis of variance for in-plane permeability perpendicular.**

Source	Sum of Squares	Degree of Freedom	Mean Square	P-value
Treatments	1.55E-09	4	3.87E-10	0.005
Experimental Error	6.69E-11	4	1.70E-11	
Observation Error	2.08E-10	116	1.79E-12	
Total	1.82E-09	124		

**Table A- 7. Analysis of variance for in-plane permeability perpendicular across all flake thicknesses.**

Source	Sum of Squares	Degree of Freedom	Mean Square	P-value
Treatments	3.70E-11	2	1.80E-11	0.011
Experimental Error	4.30E-12	4	1.10E-12	
Observation Error	2.70E-11	68	3.97E-13	
Total	6.83E-11	74		

**Table A- 8. Analysis of variance for in-plane permeability parallel and perpendicular.**

Source	Sum of Squares	Degree of Freedom	Mean Square	P-value
Treatments	6.50E-10	5	1.30E-10	0.019
Experimental Error	4.70E-11	4	1.20E-11	
Observation Error	1.70E-10	140	1.20E-12	
Total	8.67E-10	149		

**Table A- 9. Transverse permeability stepwise regression step 1 analysis of variance and the first variable entered parameter estimates.**

Source	Sum of Squares	Degree of Freedom	Mean Square	F Value	P-value
Model	2441.95	1	2441.95	2179.29	<0.0001
Error	444.85	397	1.12		
corrected Total	2886.8	398			
<b>Parameter Estimates</b>					
Variable	Parameter Estimate	Standard Error	Type II Sum of Squares	F Value	P-value
intercept	-16.12	0.074	53870	48076	<.0001
compaction <sup>3</sup>	-1.47	0.031	2441.95	2179	<.0001

Variable Compaction<sup>3</sup> entered: R-Square = 0.8459 and C(p) = 250.2

**Table A- 10. Transverse permeability stepwise regression step 2 analysis of variance and the next variable entered parameter estimates.**

Source	Sum of Squares	Degree of Freedom	Mean Square	F Value	P-value
Model	2601.5	2	1300	1805.33	<0.0001
Error	285.32	396	0.72		
corrected Total	2886.82	398			
<b>Parameter Estimates</b>					
Variable	Parameter Estimate	Standard Error	Type II Sum of Squares	F Value	P-value
intercept	-17.41	0.105	19982	27733.7	<.0001
compaction <sup>3</sup>	-1.46	0.025	2407	3341.21	<.0001
Thickness <sup>2</sup>	203.51	13.68	159.5	221.42	<.0001

Variable Thickness<sup>2</sup> entered: R-Square = 0.9012 and C(p) = 20.8165

**Table A- 11. Transverse permeability stepwise regression step 3 analysis of variance and the next variable entered parameter estimates.**

Source	Sum of Squares	Degree of Freedom	Mean Square	F Value	P-value
Model	2612.7	3	870.9	1255.1	<0.0001
Error	274.1	395	0.694		
corrected Total	2886.8	398			
Parameter Estimates					
Variable	Parameter Estimate	Standard Error	Type II Sum of Squares	F Value	P-value
intercept	-16.9	0.163	7444.8	10729	<.0001
compaction	-0.896	0.223	11.23	16.19	<.0001
compaction <sup>3</sup>	-1.23	0.062	272.21	392.3	<.0001
Thickness <sup>2</sup>	204.5	13.42	160.97	231.99	<.0001

Variable compaction Entered: R-Square = 0.9051 and C(p) = 6.5252

**Table A- 12. Transverse permeability stepwise regression step 4 analysis of variance and the last variable entered parameter estimates.**

Source	Sum of Squares	Degree of Freedom	Mean Square	F Value	P-value
Model	2615.5	4	653.9	949.8	<0.0001
Error	271.3	394	0.688		
corrected Total	2886.8	398			
Parameter Estimates					
Variable	Parameter Estimate	Standard Error	Type II Sum of Squares	F Value	P-value
intercept	-16.36	0.31	1917.8	2786	<.0001
compaction	-3.2	1.16	5.26	7.63	0.006
compaction <sup>2</sup>	2.56	1.26	2.83	4.11	0.0432
compaction <sup>3</sup>	-2.05	0.409	17.3	25.13	<.0001
Thickness <sup>2</sup>	203.99	13.37	160.2	232.69	<.0001

Variable compaction<sup>2</sup> Entered: R-Square = 0.9060 and C(p) = 4.4186

**Table A- 13. In-plane permeability parallel stepwise regression step 1 analysis of variance and the first variable entered parameter estimates.**

Source	Sum of Squares	Degree of Freedom	Mean Square	F Value	P-value
Model	7.13E-09	1	7.13E-09	1178	<0.0001
Error	9.93E-10	164	6.05E-12		
corrected Total	8.123E-09	165			
Parameter Estimates					
Variable	Parameter Estimate	Standard Error	Type II Sum of Squares	F Value	P-value
interaction	0.00007123	0.0000021	7.13E-09	1178	<0.0001

Variable interaction Entered: R-Square = 0.8778 and C(p) = 23.1508

**Table A- 14. In-plane permeability parallel stepwise regression step 2 analysis of variance and the next variable entered parameter estimates.**

Source	Sum of Squares	Degree of Freedom	Mean Square	F Value	P-value
Model	7.25E-09	2	3.63E-09	680	<0.0001
Error	8.69E-10	163	5.33E-12		
corrected Total	8.12E-09	165			
Parameter Estimates					
Variable	Parameter Estimate	Standard Error	Type II Sum of Squares	F Value	P-value
thickness	-0.0000235	0.0000049	1.23E-10	23.15	<0.0001
interaction	0.00008857	0.0000041	2.49E-09	467	<0.0001

Variable thickness Entered: R-Square = 0.8930 and C(p) = 2.0000

**Table A- 15. In-plane permeability perpendicular stepwise regression step 1 analysis of variance and the first variable entered parameter estimates.**

Source	Sum of Squares	Degree of Freedom	Mean Square	F Value	P-value
Model	3.37E-09	1	3.37E-09	1025	<0.0001
Error	5.70E-10	174	3.30E-12		
corrected Total	3.94E-09	175			
Parameter Estimates					
Variable	Parameter Estimate	Standard Error	Type II Sum of Squares	F Value	P-value
interaction	0.00004793	0.000015	3.37E-09	1025	<0.0001

Variable interaction Entered: R-Square = 0.8549 and C(p) = 72.4137

**Table A- 16. In-plane permeability perpendicular stepwise regression step 2 analysis of variance and the next variable entered parameter estimates.**

Source	Sum of Squares	Degree of Freedom	Mean Square	F Value	P-value
Model	3.53E-09	2	1.77E-09	759	<0.0001
Error	4.03E-10	173	2.33E-12		
corrected Total	3.93E-09	175			
Parameter Estimates					
Variable	Parameter Estimate	Standard Error	Type II Sum of Squares	F Value	P-value
thickness	-0.00002725	0.0000032	1.69E-10	72.41	<0.0001
interaction	0.00006832	0.0000027	1.47E-09	637	<0.0001

Variable thickness Entered: R-Square = 0.8977 and C(p) = 2.0000